International Journal of Hydrogen Energy 49 (2024) 1444–1460

Contents lists available at ScienceDirect

International Journal of Hydrogen Energy

journal homepage: www.elsevier.com/locate/he

Direct reduction of pellets through hydrogen: Experimental and model behaviour

Pasquale Cavaliere [a,*], Angelo Perrone [a], Leandro Dijon [b], Aleksandra Laska [c], Damian Koszelow [d]

[a] Department of Innovation Engineering, University of Salento, Via per Arnesano, 73100, Lecce, Italy
[b] VALE, Route de Pallatex 29 St-Prex, 1162, Losanna, Switzerland
[c] Faculty of Mechanical Engineering and Ship Technology, Gdansk University of Technology, Narutowicza 11/12, 80-233, Gdańsk, Poland
[d] Advanced Materials Centre, Faculty of Electronics, Telecommunications and Informatics, Gdańsk University of Technology, ul. G. Narutowicza 11/12, Gdańsk, 80-233, Poland

ARTICLE INFO

Handling editor:Dr F Gallucci

Keywords:
Direct reduction
Hydrogen
Kinetics
Entropy
Processing parameters
Metallization degree

ABSTRACT

This paper presents the hydrogen reduction behaviour of industrial pellets designed for the efficient hydrogen based direct reduction. The pellets were provided with very low non ferrous oxides percentage (0.52 of basicity index) and with the absence on TiO_2 oxides. The pellets measured diameters in the range 1.14–1.72 cm and were characterized in terms of porosity, pores size, tortuosity and compression strength. The pellets were reduced in hydrogen atmosphere in a laboratory shaft furnace in the temperature ranges of 600–1200 °C at the pressures of 1 and 5 bar. The pellets' reduction behaviour was analysed in terms of time to reduction, rate of reduction and kinetics constant. All the obtained results were analysed through the employment of a commercial multi-objective optimization tool (modeFrontier) in order to precisely define the effect of each single parameter on the pellets' reduction. It was also defined the effect of the ongoing reduction rate of the final metallization of the starting iron oxides.

1. Introduction

Many evolutions are going to be faced by the ironmaking and steelmaking industries at the present times and other important revolutions are expected to be faced in the very next future. These changes are due to the fundamental aspect that the traditional integrated route has always been accompanied with high levels of green house gases emissions. In 2021, the global steel production accounts for 1951 million tons (Mt) where the traditional blast furnace-basic oxygen furnace covers the 70 % of the overall crude steel [1].

Per each ton of crude steel, 1.8 ton of carbon dioxide is produced with the traditional integrated route. Now, given the continuous growing of the global steel production, the greenhouse gases emissions are destined to grow if only the integrated route is retained as production technologies. Given all this, the only way to reduce dangerous emissions is the deep application of the so-called best available techniques (BAT) [2].

Among BAT, direct reduction (DR) is considered the most advanced technology to reduce the emissions during the primary ironmaking production. Green hydrogen technology has the potential to reduce the carbon dioxide emissions from iron and steelmaking to nearly zero and mitigate climate change from the industrial sector [3]. Globally, the most employed technologies are based on shaft furnaces of the type Midrex and HYL [4,5].

Here, the processes were designed to employ syngas as the main reducing agent but remarkable differences in the plants configurations can be underlined [6]. This is driven by the aspect that many inconveniences must be managed for the optimal reduction kinetics of iron oxides in the $CO–H_2–CO_2–H_2O$ atmosphere generated in the shaft furnace [7,8]. This is because potential kinetics decelerations could lead to very high gas consumptions with consequent high energy needing for the overall oxides reduction [9,10]. The precise understanding of the pellets reduction behaviour as a function of the gas composition and processing parameters is fundamental to increase the overall process efficiency accompanied with high quality of the produced material [11]. Depending on the reducing atmosphere and temperature, the performance of the technology, such as the reduction rate, metallization degree, and behaviour of the iron ore, can be significantly modified [12].

All these variables conduce to important complications in the development of affordable models capable of providing robust

* Corresponding author.
E-mail address: pasquale.cavaliere@unisalento.it (P. Cavaliere).

https://doi.org/10.1016/j.ijhydene.2023.11.040
Received 10 April 2023; Received in revised form 29 October 2023; Accepted 3 November 2023
Available online 11 November 2023

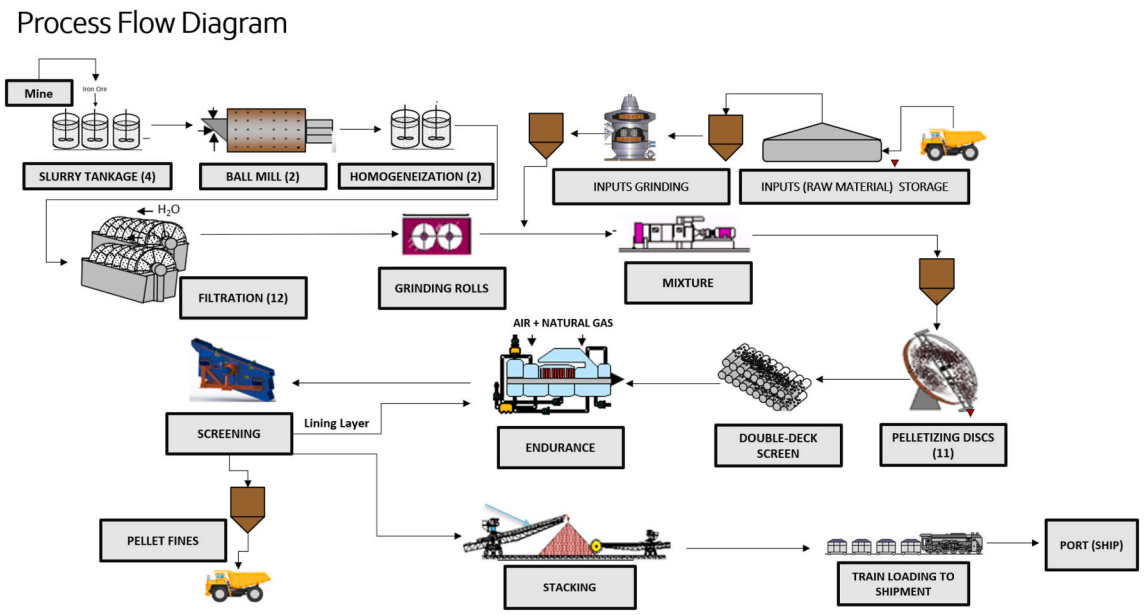

Fig. 1. Pellets production flow diagram.

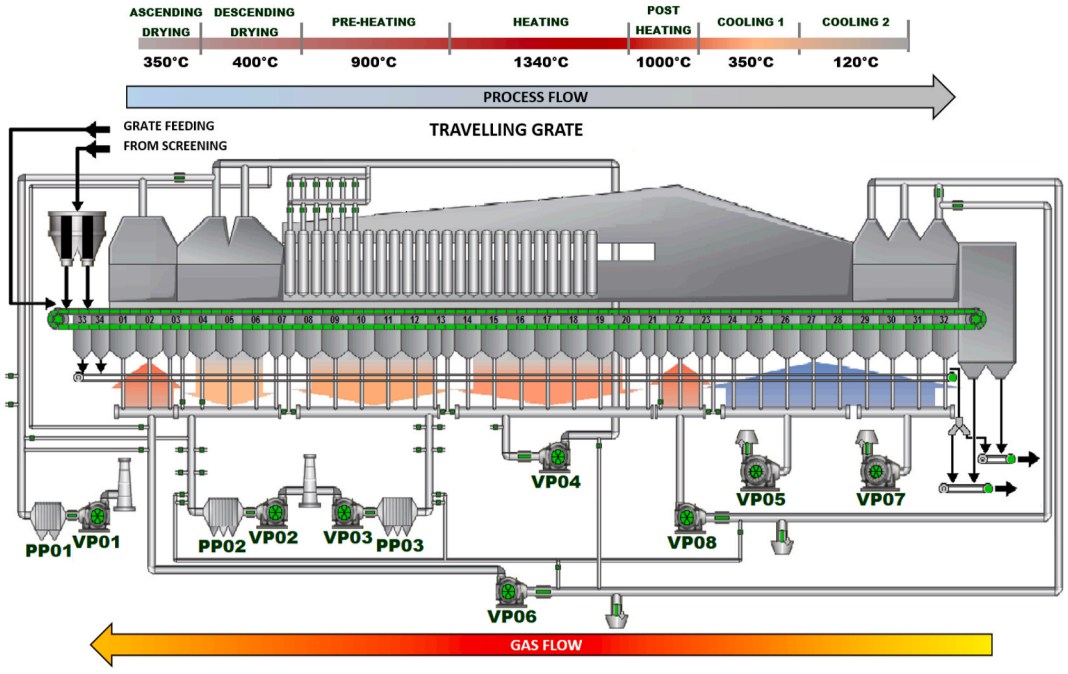

Fig. 2. Endurance procedure schematic with (in scale) the indication of the different stage temperatures. PP=Precipitator, VP=Vacuum Pump.

previsions for the precise reduction of iron oxide pellets in various compositional, physical and processing conditions [13,14].

Most of the models available in the scientific literature focus on the direct reduction through a gas mixture of hydrogen and carbon monoxide. This leads to a simplification of all the thermo-chemical and thermo-physical phenomena developing during the reduction stages [15–17].

During the direct reduction processes, the gases lead to the transformation of iron oxide pellets to elemental iron enriched with the metals of the previously incorporated oxides. The final reduced material is known as directly reduced iron (DRI). The reducing gases are typically hydrogen and natural gas leading to H2+CO reducing atmosphere. The generation of this gas occurs through methane reforming, which can be done in a reformer or inside the reduction shaft with the sponge iron as a catalyst [18]. By moving to the direct reduction based on only hydrogen atmosphere, this allows to have a carbon free process with only water vapor as by-product [19]. This allows for the total carbon free primary ironmaking process [20]. Some evidences underline that carbon-negative steel production can be achieved [21]. Hydrogen can be produced by various technologies with excellent efficiency [22]. Obviously, the energy balance is fundamental in the analyses of the transition toward new steelmaking routes [23]. So, obviously the costs of transition have a large impact on the applicable best available technologies [24], and the defossilization of steel production needs further deep studies and complex alanyses [25].

Hydrogen is actually extensively studied as a reducing agent in many

Fig. 3. Customized shaft furnace.

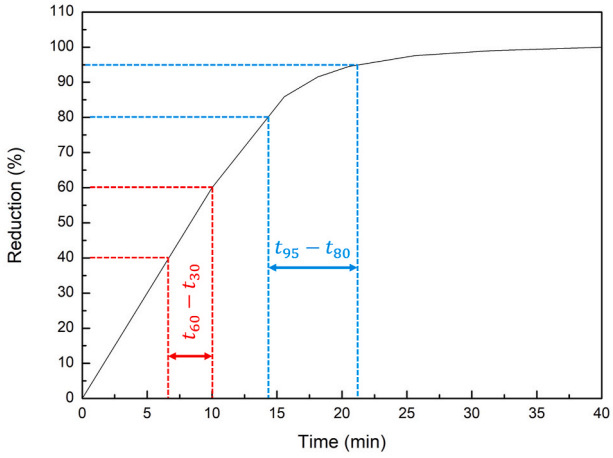

Fig. 4. Rates of reduction indexes calculation.

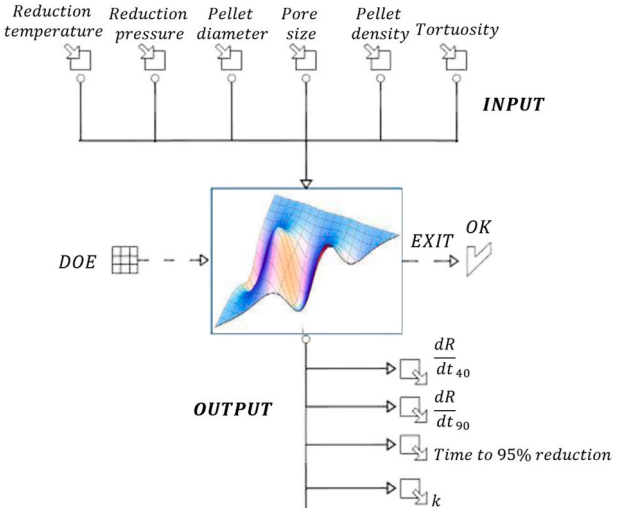

Fig. 5. Description of the Workflow indicating the correlation between input and output.

Table 1
Pellets composition.

TFe (%)	CaO (%)	Mn (%)	Al_2O_3 (%)	SiO_2 (%)	P (%)	MgO (%)	S (%)
67.24	1.02	0.144	0.38	1.97	0.031	0.63	0.018

Fig. 6. Different pellets employed in the present study.

primary metallurgical processes [26].

The hydrogen-based direct reduction process includes multiple types of chemical reactions, solid state and defect-mediated diffusion (of oxygen and hydrogen species), several phase transformations, as well as massive volume shrinkage and mechanical stress buildup [27]. By considering the physical modifications, during reduction the pellets volume increases and some crucial swelling phenomena could cause abnormal reduction leading to a decrease in the pellets permeability and in some cases to the collapse of the burden [28]. For these reasons, the swelling behaviour of the starting pellets must be carefully characterized [29]. Now, swelling occurs during the transformation of wustite into iron. During this phenomenon, limited nucleation occurs, and these nuclei grow like needles causing a volume increase, which is seen as swelling This coincides with a low compression strength of this structure, with the opportunity to generate fines. Anyway, Pellets in H_2 rich atmosphere passed the wustite stage rapidly and swelling is consequently weakened.

Hydrogen-based direct reduction reveals complex physical-chemical-mechanical interactions leading to very complex reduction mechanisms characterized by on-going steps with respect to mass transport and volume modifications [30]. The different oxides transformations are characterized by very different rates with kinetics behaviour of order of magnitudes in the reduction times all influencing the final pellets metallization [31].

Replacing carbon in ironmaking processes requires a deeper understanding of the kinetics of iron oxide reduction in order to provide crucial elements for selecting the best-operating conditions and designing new technologies [32].

Many are the analytical models described in the literature on the kinetics behaviour during direct reduction processes taking into account the physical and processing parameters governing the overall process [33,34]. So, the reduction process is influenced by the shaft furnace environment (gas composition, temperature and pressure) and by the pellets properties (composition, density, pores size, pores tortuosity) [35,36]. All these very different parameters often falling in very broad ranges lead to the uncertainty of many presented results. For all these reasons, many models present a balance between simple development and acceptable accuracy that can give results comparable with the experimental evidences [37,38].

The scientific attention on the direct reduction processes has continuously grown in the recent past. This was also due to the industrial needing for greenhouse gas reduction as well as to the prices peaks for the reforming of natural gas [39].

So, the precise behaviour of the reactions kinetics of direct reduction of industrial pellets has immediate consequences on the process

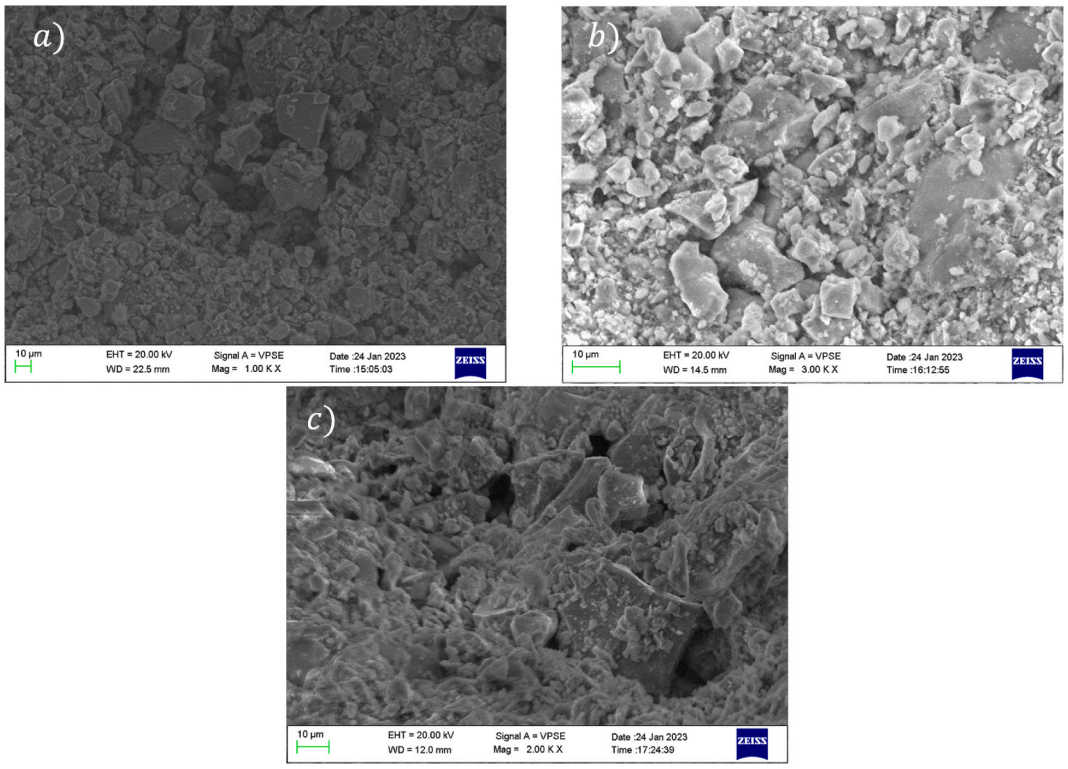

Fig. 7. Surface pellets aspect: a) 1.72 cm in diameter, b) 1.36 cm in diameter and c) 1.14 cm in diameter.

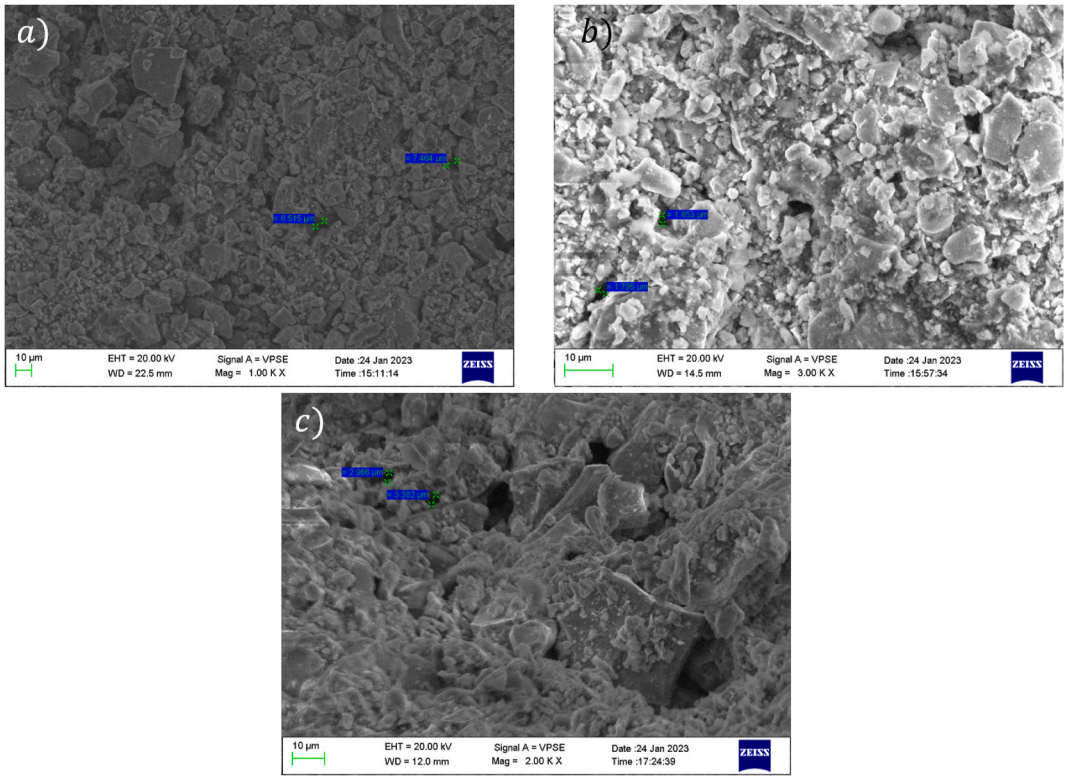

Fig. 8. Surface pores measurements: a) 1.72 cm in diameter, b) 1.36 cm in diameter and c) 1.14 cm in diameter.

performances of high volume of treated oxides [40,41]. In addition, the starting pellets properties and the processing conditions influence the final product characteristics and the further melting operations in terms of melting temperatures and slag formation [42].

Generally, hydrogen-based direct reduction allows for the fastest transformation of industrial pellets, the time to reduction results increased in the case of the employment of a carbon monoxide atmosphere with intermediate reduction times in the case of these two gases

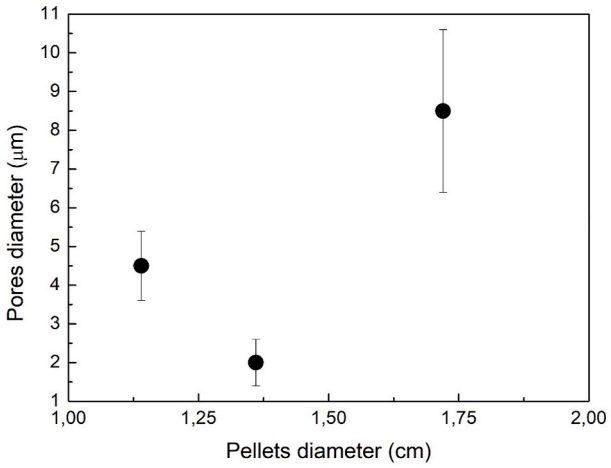

Fig. 9. Statistical analyses of surfaces pores size.

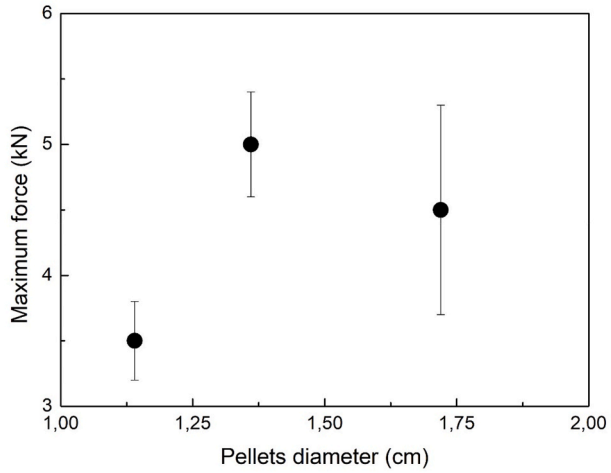

Fig. 10. Maximum force exhibited during the compression tests of the pellets as a function of the pellet diameter.

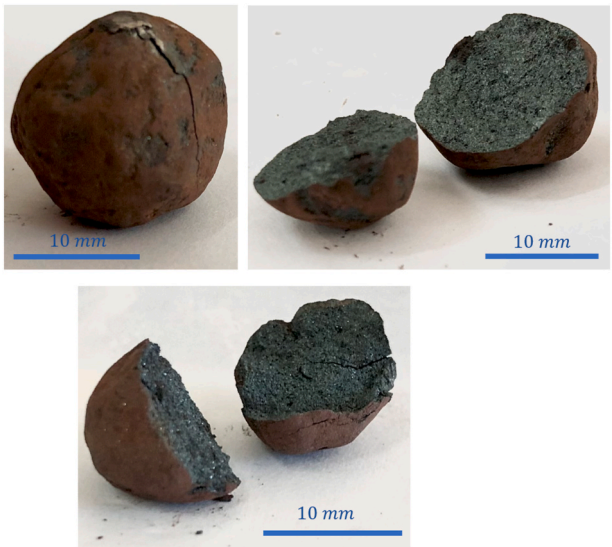

Fig. 11. Pellets aspect after the compression tests.

mixing; obviously the trend is not linear [43]. The employment of a given gas type leads to strong modifications in the overall energy consumption of the process [44]. This is deeply related to the molecular dimensions of the reducing gases and to their diffusion inside the pellets. This obviously at the same level of temperature whose increase leads to the acceleration of the reduction phenomena [45]. In the case of employment of gas mixtures, the kinetics increase as the temperature and the hydrogen content in the gas mixture increase [46].

As a matter of fact, the addition of hydrogen leads to the process acceleration. Even if, the hydrogen production is high energy expensive and it produces many variations in the thermodynamic behaviour of the reduction process because of the development of endothermic reactions. So, large volumes and high pressures are needed to overcome the heat losses [47,48]. In fact, hydrogen based direct reduction is endothermic, whereas with carbon monoxide the reduction is exothermic. Above 800 °C, however, thermodynamics are more favourable with hydrogen than with carbon monoxide, where the reduction rate with H_2 is much higher than the case with CO at 850 °C.

Many papers are presented in the literature on the hydrogen direct reduction of iron ore fines with accepted general consensus on the main results [49]. On the contrary, in the case of industrial pellets, results are sometimes incoherent especially with respect to the precise kinetics behaviour for different type of pellets reduced in various temperature and pressure conditions. As a matter of fact, the starting pellets composition, the pellets density and the pores dimensions and shape have large influence on the reduction behaviour. So, a final agreement on the effect that all these aspects have on the process development has not been achieved yet. As a results, many discrepancies can be underlined in the available literature also because many experimental evidences are related to just one type of pellets in terms of composition and porosity [50].

Another important industrial aspect is that sponge iron generally requires a carbon content in the range 1.5–4.5 % that is fundamental for the further melting operations. Now, the pellets reduced via pure hydrogen are carbon free leading to an increase in the melting temperature of the sponge iron (1538 °C). As a consequence, carburization is needed [51,52]. DR under CO atmosphere is often accompanied by carbon deposition due to an inverse Boudouard reaction at temperatures <1000 °C.

The direct reduction reaction are chemically non-catalytic solid-gas reactions. During the process, as the chemical reactions between the gas and the different kind of metal oxides occur many structural modifications in the pellets take place [53]. Actually, as the structural changes take place, the further interaction with the unreduced structure changes leading to modifications in the gas solid reactions [54]. All this dynamic behaviour leads to complications in the precise analytical analyses of the overall reduction process. This aspect is described in the results and discussion section where we tried to correlate the different stages of the reduction process by analysing the numerical behaviour of the reducing indexes at different stages of the reduction.

For a global understanding of the reduction behaviour of the industrial pellets, the complexity results increased because of the variability of composition, pellets dimensions and porosity [55].

In addition, many can be the rate limiting steps of the overall process. The nature of these limiting steps can be diffusive, chemical or both leading to different microscopic reduction phenomena. This depends on the pellets properties such as porosity and pores geometry, density, size, oxides composition and by the employed processing conditions in terms of gas mixing, gas pressure and temperature and flow rate [56].

The hematite reduction in hydrogen atmosphere follows these steps: Fe_2O_3–Fe_3O_4–FeO–Fe. In the case of industrial pellets the chemical transformations of the oxides are not the only limiting steps of the process. For this reason, many kinetics parameters are presented in literature as belonging to the Arrhenius type behaviour. This can lead to confusions in the industrial set-up of the shaft furnaces operations.

During the direct reduction of porous industrial pellets through

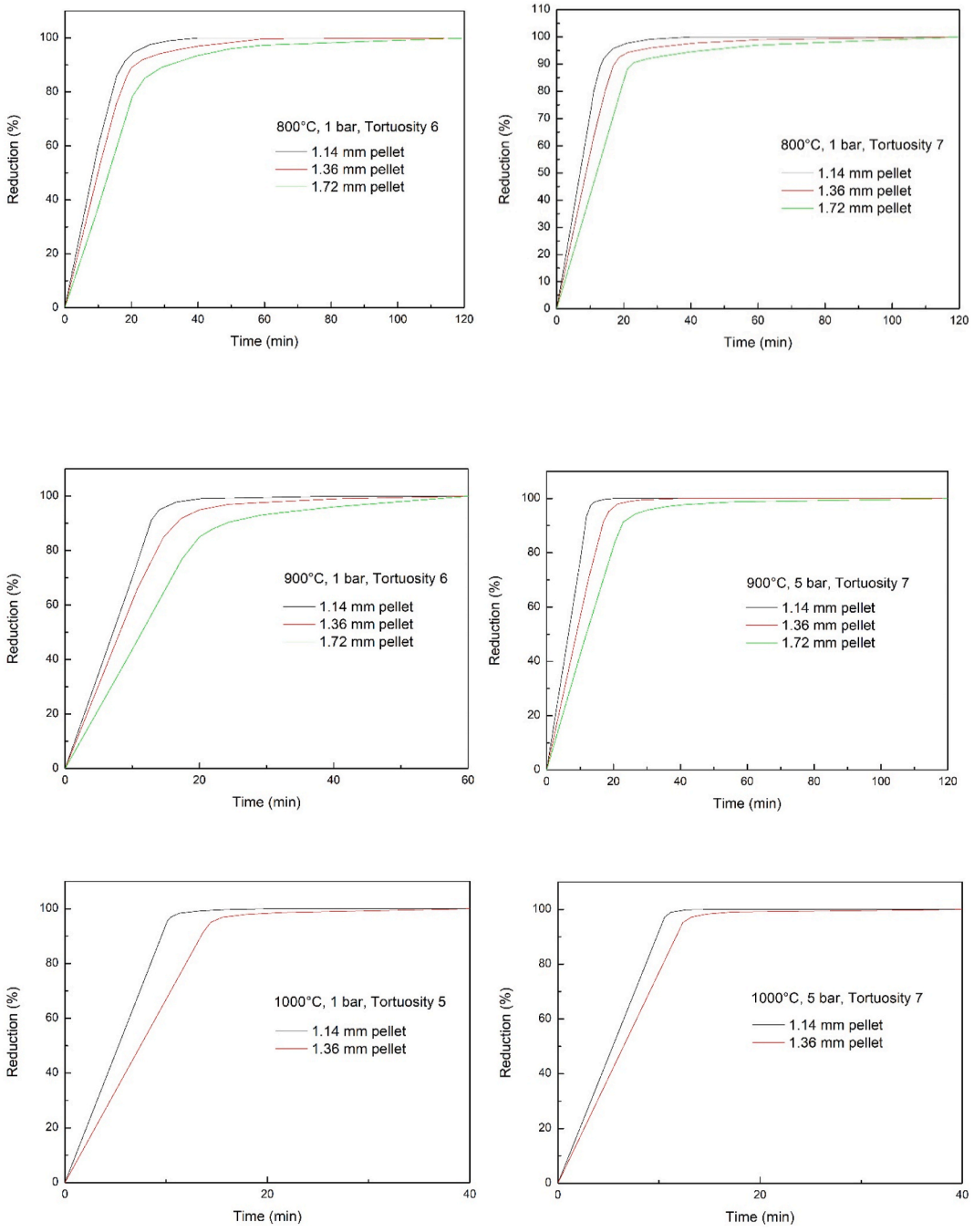

Fig. 12. Reductio percentage vs. reduction time in different conditions of temperature, pressure and pellets tortuosity.

hydrogen the following main steps can be taken into account.

- mass transfer of the hydrogen from the stream to the surface of the pellets,
- diffusion of the approaching gas through the tick film surrounding the pellet,
- diffusion inside the surface pores,
- adsorption of hydrogen at the different oxides interphases,
- consequent oxygen removal through phase boundary reactions,
- formation of water vapor, iron oxides and ferrous iron,
- desorption of all the gases belonging to the reactions,
- solid state diffusion of the reacted products,
- diffusion of gaseous products back toward the pellet surface,
- mass transfer of the gaseous product toward the stream.

They are all interconnected and so further steps can be largely influenced by the previous taking place ones.

Given all these phenomena, the main factor influencing the process is the pellets porosity in terms of dimensions, tortuosity and pores distribution. This is related to the specific hydrogen volume reacting with the pellet internal surface. This is why, in the case of low porosity and low surface pores dimensions, the gas finds many obstacles to penetrate inside the pellet. In this case, the solid state diffusion from the surface starts to become more important but it results different orders of magnitude slower than the gas diffusion. So, all the chemical reactions are driven by the hydrogen adsorbed at the pellet surface [57].

As well-known, the chemical reactions kinetics depend on the temperature levels. As the reduction temperature decreases, the chemical reactions start to be the overall rate limiting step. As the temperature

Fig. 13. Pellets reduced in hydrogen at 1000 °C.

increases, the dependence is exponentially dependent on the reduction rate and can be easily described by the Arrhenius equation (Eq. (1)):

$$k = Ae^{-\frac{E_a}{RT}} \quad (1)$$

where k is the kinetic constant, A is the Arrhenius constant, Ea is the activation energy, R is the universal gas constant and T is the absolute temperature.

So, as the temperature increases, the rate-limiting step is represented by the mass transfer. This is why the chemical reactions tend to be faster with respect to the transport of reactants and reactions by-products [58, 59].

Here, the effective diffusion coefficient is influenced by the gas physical properties and by the temperature. As both temperature and hydrogen content are increased, the diffusion coefficient increases. With respect to the carbon monoxide reduction, hydrogen-based reduction effective diffusion coefficient is higher because of the reduced molecular dimension.

Another difference with respect to the carbon monoxide reduction is that in the case of hydrogen based direct reduction pressure is fundamental for the increase of the reduction rate. As a matter of fact, in the industrial shaft furnaces from HYL, the reactor pressure is close to 8 bar in order to reduce the volatility of the reducing gas [60].

Another aspect resulting as fundamental for the direct reduction behaviour is the pellet composition in terms of iron oxides, different metals oxides, gangue and impurities. Obviously, the reduction rate is largely influenced on the oxides percentage and on their type [61]. The oxides present in the industrial pellets are typically CaO, TiO_2, SiO_2, Al_2O_3, MnO, MgO. Normally the content of alumina largely influences the reduction rate. The so-called basicity index (normally calculated as the rate CaO/SiO_2) largely influences the reduction rate, the swelling behaviour and the pellets strength [62]. The pellets strength can be efficiently controlled through the employment of proper binders during the pelletizing procedure [63].

Another fundamental aspect is that porosity tends to increase as the reduction processes take place. This phenomenon tends to lead to an acceleration of the reaction kinetics as the reduction process advances.

Given that the diffusion can be the rate-limiting step, porosity and pores dimensions have a remarkable influence on the reduction process. This is due to the fact that both porosity and pores size influence the specific area of the pellets then defining the available surface for the reactions development. This aspect is crucial and must be precisely defined in a model that would soundly describe the evolution of these systems.

The tortuosity factor of the pores is another remarkable parameter. This influences the gas path and so the rate of the gas-oxides interaction. When the tortuosity factor increases, the gas flow is more and more turbulent, so, as the tortuosity increases, the reduction rate decreases [64]. Both porosity and tortuosity depend on the pelletizing procedure. Tortuosity can vary in the range 1–10 even if the main pelletizing procedures allow to obtain tortuosity in the range 2–6.

The aim of the present paper is the description of the kinetics behaviour of industrial iron oxide pellets during the hydrogen based direct reduction. The experimental-numerical investigations are finalized to the definition of the effect that each single parameter (pellets properties and processing conditions) has on the overall reduction behaviour of each single pellet. In addition, an analyses of the intermediate reducing conditions on the further reduction behaviour was provided.

2. Experimental procedure

2.1. Mining and pelletizing procedure

The studied pellets were provided by VALE (Brazil). The pelletizing flow diagram is shown in Fig. 1.

The iron ore pelletizing plant begins with the grinding process, where the ore is mixed with a specific solid content and grinding balls of varying sizes. The plant has multiple ball mills, each with a considerable capacity to process the ore. The quality parameter during this stage refers to the Specific Surface (blaine), with a usual target ranging from 1500 to 1,600cm2/g. Once the grinding is completed, the material undergoes vacuum filtering. The filters used in this process are large in diameter and provide a significant filtering area. After the filtering stage, the material is subjected to High Pressure Grinding Rolls (HPGR), which further refines the quality parameters. The HPGR process has a notable capacity and uses rolls with specific dimensions in diameter and width.

Table 2
Weight variation for different pellets reduced at 950 and 1000 °C at various times.

Temperature (°C)	Reduction time (min)	Initial diameter (cm)	Final diameter (cm)	Initial mass (g)	Final mass (g)	Mass variation (%)
950	90	1,36	1,18	3,98	2,83	29
950	90	1,3	1,2	3,98	2,83	28,9
950	90	1,46	1,41	5,65	4	28,6
950	90	1,5	1,41	5,9	4,2	28,9
950	90	1,85	1,72	10,49	7,43	29,1
950	90	1,8	1,74	10,1	7,23	28,6
1000	90	1,37	1,17	4,08	2,88	29,36
1000	90	1,74	1,6	9,32	6,53	29,92
1000	30	1,62	1,51	7,83	5,56	29
1000	30	1,4	1,3	4,3	3,06	28,9
1000	5	1,4	1,3	4,3	3,1	28,8
1000	5	1,43	1,32	5	3,55	28,8
1000	20	1,29	1,15	3,68	2,6	28,95
1000	20	1,55	1,41	6,1	4,3	28,9
1000	20	2	1,87	13,7	9,76	28,9

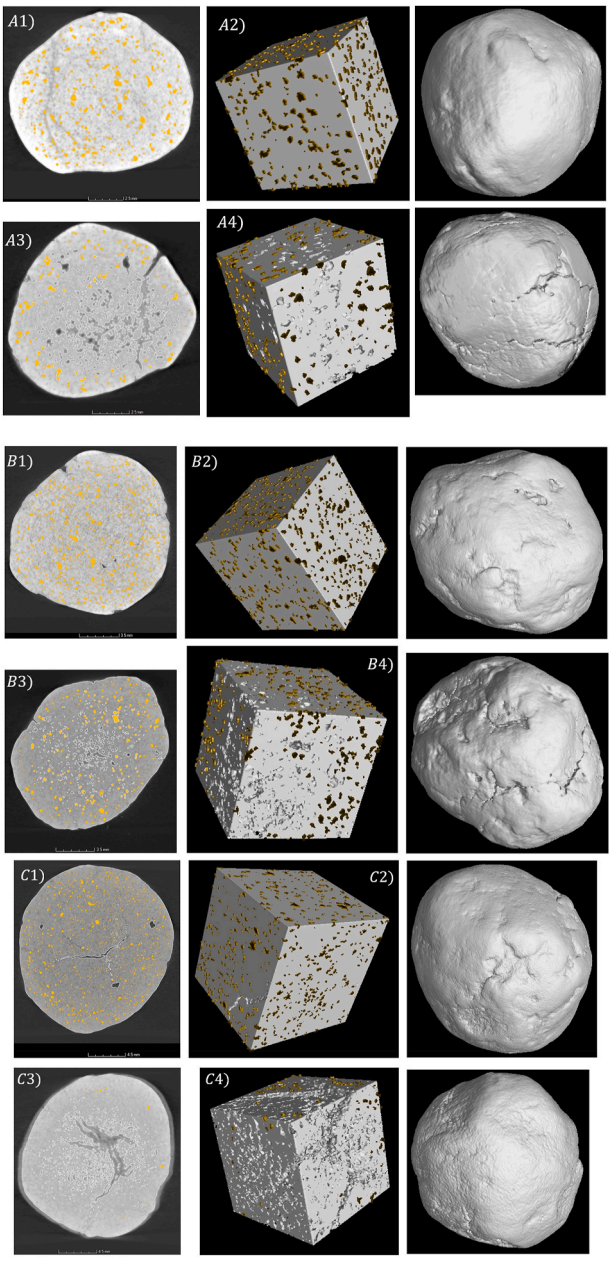

Fig. 14. Microtomography observation of the pellets before and after reduction at 1000 °C in pure hydrogen, A1, A2 1,14 cm in starting diameter unreduced, A3, A4 1,14 cm starting diameter reduced; B1, B2 1,36 cm in starting diameter unreduced, B3, B4 1,36 cm starting diameter reduced; C1, C2 1,72 cm in starting diameter unreduced, C3, C4 1,72 cm starting diameter reduced.

Finally, the material is sent to the pelletizing discs, which have a wide range of capacities per disc. The plant features multiple discs, with both discs and screens having specific dimensions in diameter and width. Then the material is subjected to the endurance processing with the procedure schematized in Fig. 2.

Finally, the pellets are filtered in order to eliminate fines (<5 mm). This comprehensive process ultimately leads to the production of iron ore pellets, providing an essential resource for various industries.

2.2. Characterization procedure

The composition of the pellets was measured through EDS in a Zeiss EVO 60 scanning electron microscope. The pellets density was measured by taking seven diameters of the pellets and after the average diameter

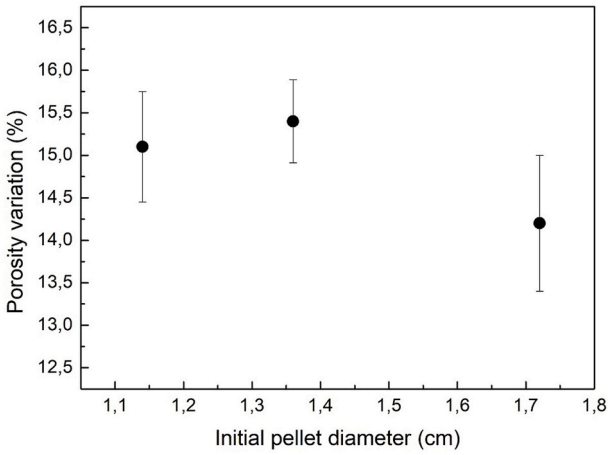

Fig. 15. Porosity variation after reduction as a function of the starting diameter of the analysed pellets.

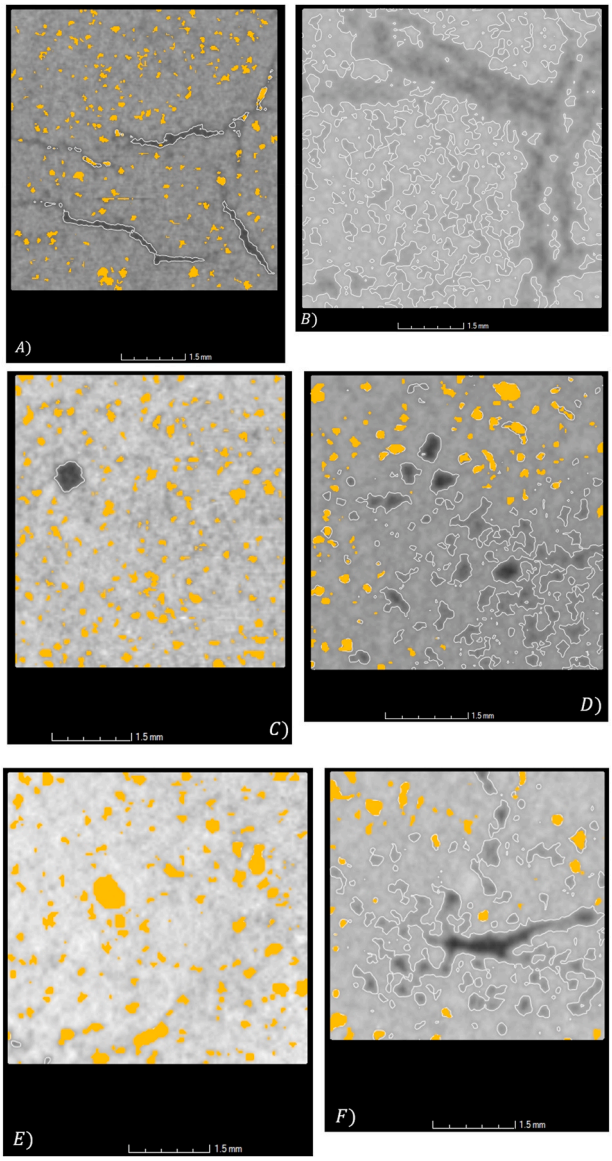

Fig. 16. Pores aspect for the pellet with starting diameter of 1,72 cm before A) and after B) reduction; 1,36 cm before C) and after D) reduction; 1,14 cm before E) and after F) reduction.

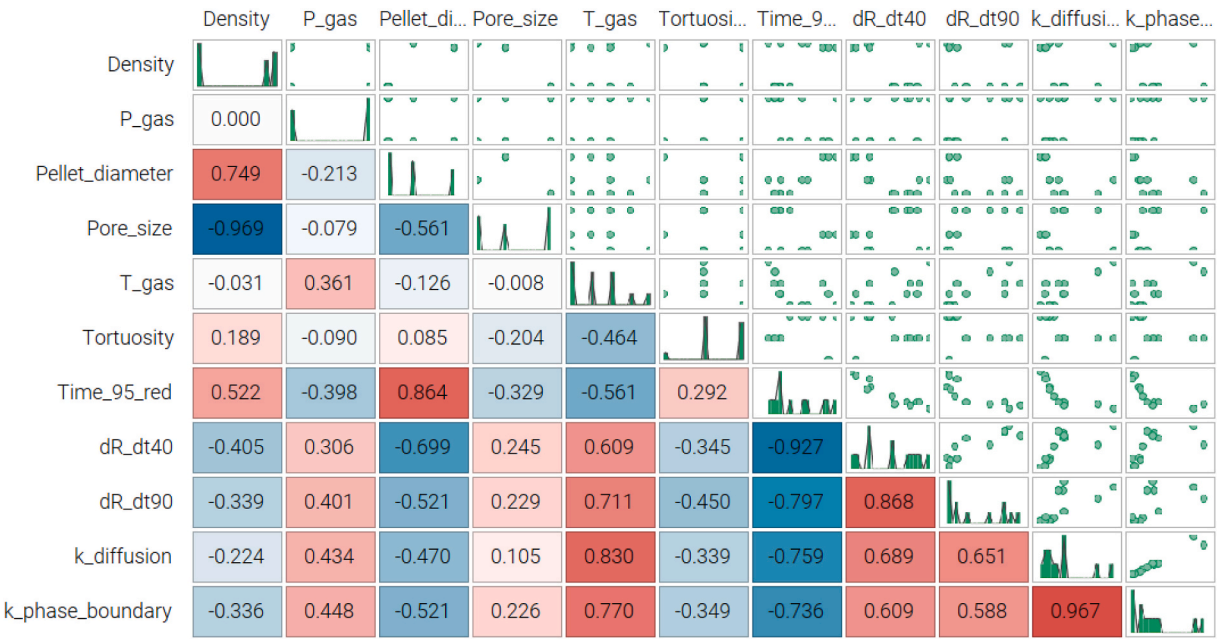

Fig. 17. Scatter matrix of the hydrogen direct reduction of the VALE pellets.

calculation, this was used to calculate the density after weighing the pellets with a precision balance (resolution 0.0001 g). The surface microstructure of the pellets was analysed with Scanning electron microscope in order to measure the surface pores.

The compressive strength of the pellets was evaluated with a Zwick/Roell Z100 standard testing machine at the speed of 0.5 mm/min. The pellets reduction experiments were performed in an in-house designed and developed shaft furnace shown in Fig. 3.

The direct reduction experiments were carried out in the temperature range of 600–1200 °C with 100 °C of delta. The gas composition was 100 % H2 hydrogen. The employed hydrogen pressures were 1 and 5 bar. The reduction hydrogen flow was set at 160 ml per minute. The pellets starting diameter and the pellets mass were measured before and after the reduction. The pellets porosity was analysed by microtomography by employing a Phoenix v/tome/x s (General Electric).

From the reduction curves (reduction percentage vs. time to reduction) they were calculated the kinetics constants and the rates of reduction.

The kinetic constant was calculated through the three dimensional diffusion model (Eq. (2)):

$$k = \frac{\left[1-(1-\alpha)^{\frac{1}{3}}\right]^2}{t} \tag{2}$$

and through the three dimensional phase boundary controlled reaction (Eq. (3)):

$$k = \frac{1-(1-\alpha)^{\frac{1}{3}}}{t} \tag{3}$$

where α is the fraction reacted (0–1) and t is the time at which a given fraction of the material reacts [65].

The reduction rate is analysed through the definition of two indexes described in Equations (4) and (5):

$$\frac{dR}{dt}_{40} = \frac{33.6}{t_{60}-t_{30}} \tag{4}$$

$$\frac{dR}{dt}_{90} = \frac{13.9}{t_{95}-t_{80}} \tag{5}$$

with t_{95}, t_{80}, t_{60} and t_{30} being the time required to reduce the pellets by 95, 80, 60 and 30 %. This is schematized in Fig. 4.

The employed databases are attached as supplementary material.

2.3. Modelling procedure

The data belonging to the reduction experiments in terms of pellets properties, processing parameters and results were analysed through the multi-objective software modeFrontier. It allows to obtain the so called "Pareto Frontier" that is known as the best trade-off between all the objective functions. modeFRONTIER's optimization algorithms identify the solutions which lie on the trade-off Pareto Frontier. This allows for the identification of the best possible solutions that become the optimal solutions. The analyses performed through modeFrontier goes through the gradient methods where the algorithms search for either the minimum or the maximum of an objective function, depending on the goal. So, the first important result to be gained is the suitable weighted effect of each considered single input parameter on a given output. So, this immediately allows to determine which are the most effective parameters influencing the studied process.

This allows also to separate the objectives in the case of the optimization step. Naturally, in the case of very complex analyses (many inputs and many outputs) the optimization will result a deep compromise among many potential optimal solutions. So, the final optimization algorithm will present many results lying on the trade-off Pareto Frontier. These solutions all have the characteristic that none of the objectives can be improved without prejudicing another [66,67]. The software offers wide-ranging toolbox, allowing the user to perform sophisticated statistical analysis and data visualization. It provides a strong tool to design and to analyze experiments, it eliminates redundant observations and reduces the time and the resources to make experiments. In our previous experiences, the software was very successfully applied to the analyses of ironmaking and steelmaking processes [68–70].

Starting from a database built with experimental results, computational models were developed (virtual n-dimensional surfaces) able to reproduce at best the actual process. The method used for the creation of meta-models to simulate the actual process through the use of physical laws with appropriate coefficients to be calibrated was that of the response surfaces (RS). This method consists of creating n-dimensional surfaces that are "trained" on the basis of actual input and output. These

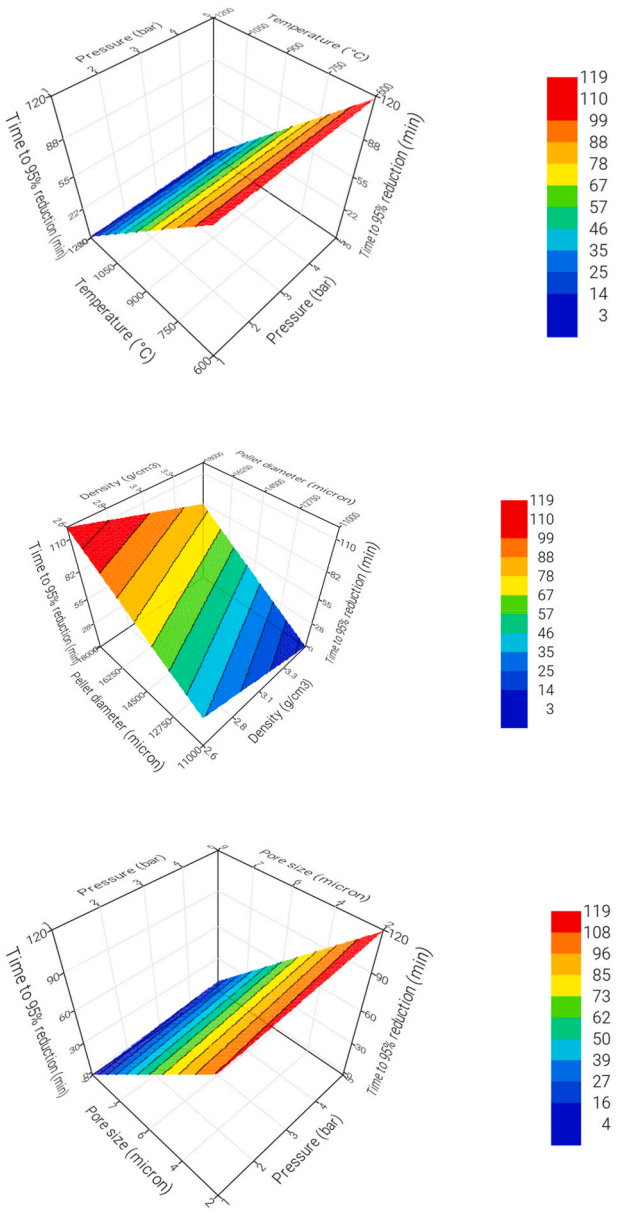

Fig. 18. Time to 95 % reduction as a function of the different input parameters.

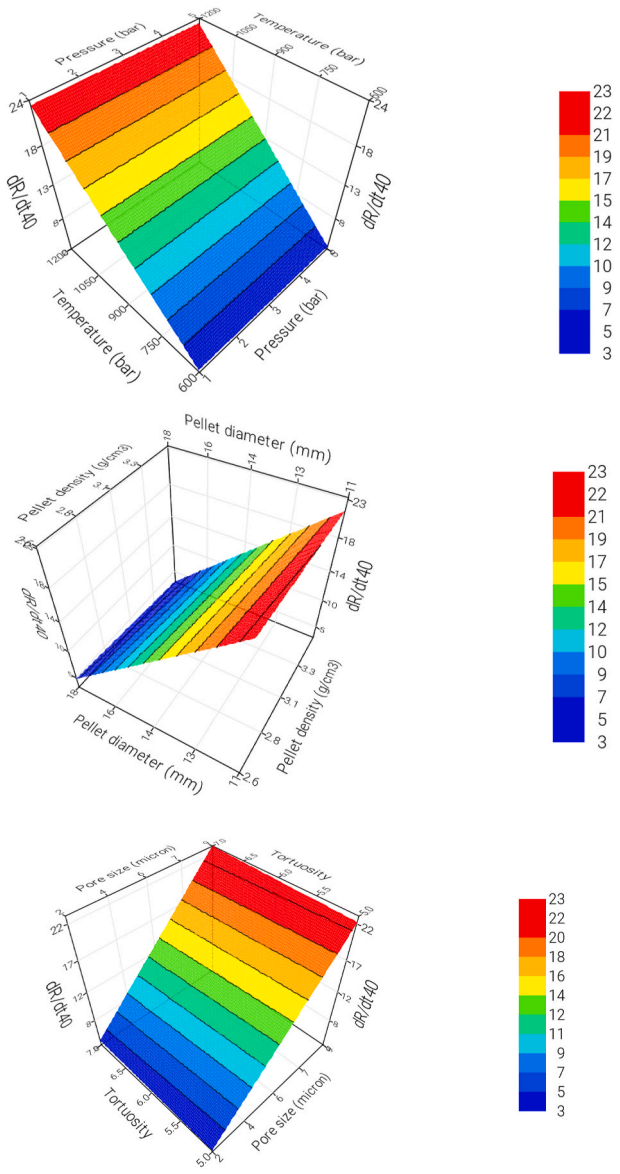

Fig. 19. dR/dt40 as a function of the different input parameters.

surfaces trained on a large experimental data can give the output numbers that reflect the real process.

The reduction process through the analysis performed by Mode FRONTIER is summarized in the Workflow of Fig. 5.

The workflow is divided into data flow (solid lines) and logic flow (dashed lines) that have the computer node as their common node. Here physical and mathematical functions representing the reduction process are introduced. In the data flow all input parameters optimized in the numerical simulations are included.

- Reduction temperature,
- Reduction pressure,
- Pellet diameter,
- Pores size,
- Pellet density,
- Tortuosity factor, and those outputs:
- kinetic constant (k),
- reduction rates (from equations (4) and (5)),
- Time to 95 % reduction.

These were used to define the so-called scatter matrix where immediately the weight of each input on the variation of a given output is numerically defined between −1 and +1. If the correlation factor is −1 it means that the input and the output are perfectly inversely proportional. On the contrary, if the correlation factor is +1, the input and the output are perfectly directly proportional.

3. Results and discussion

By reducing iron oxides through hydrogen, the rate of chemical reactions and consequently the reduction speed increases with respect to the traditional natural gas-based processes. The employed pellets had a composition listed in Table 1.

Iron content is high revealing the good quality of the pellets. This will allow to produce more steel with the same raw materials volumes. In addition, the time for the direct reduction can be reduced by largely influencing the energy consumption of the overall process [71]. Binary basicity is also known as a factor for controlling the swelling index [72], as pellets with high swelling are prone to generate fines during the reduction and disturb the overall process and material flow.

The basicity index of the pellets resulted to be 0.52. The composition

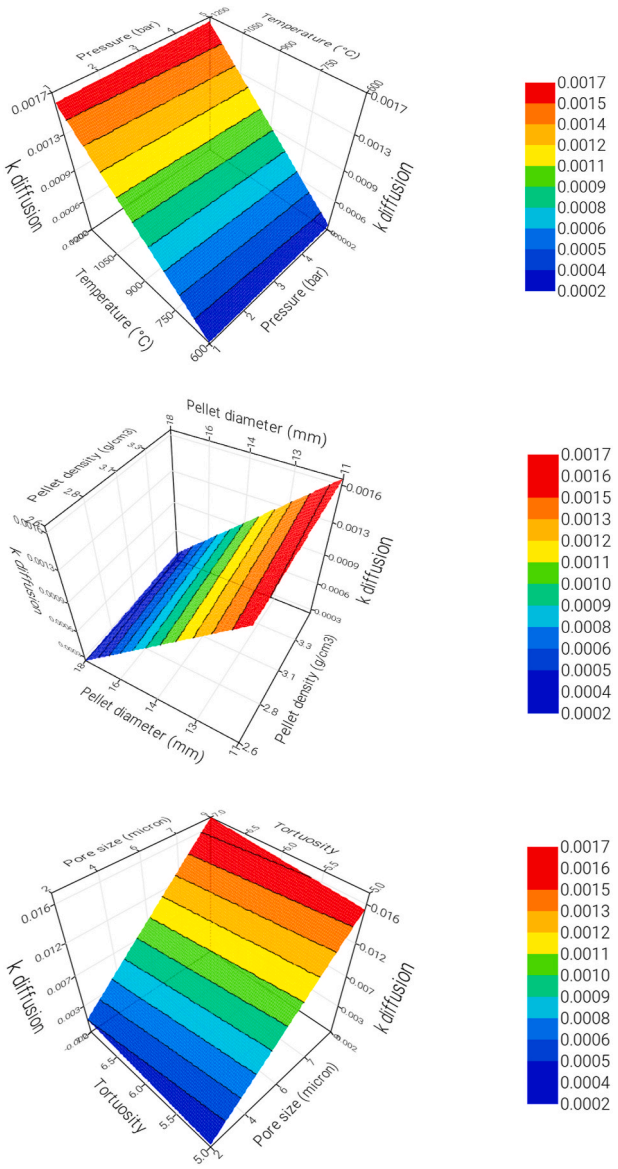

Fig. 20. k three dimensional diffusion as a function of the different input parameters.

of the pellets largely influences the reduction behaviour. In particular, the basicity index is related to the time to reduction. In general, it tends to decrease as the basicity index decreases up to a minimum time to reduction for a basicity index close to 1, then the time to reduction tends to increase as the basicity index increases [71]. It is suggested that the basicity index should be retained at an appropriate level in order to reduce the time for the reduction of the pellets. In addition, in the case of basicity index close to 1, complex calcium ferrite compounds are detecting limiting the reduction behaviour [73]. This aspect is emphasised in the case of a huge quantity of CaO. The presence of this oxide is also related to the brittleness of the pellets that can lead to difficulties in the handling and in the optimal positioning of the pellets in the shaft furnaces [74]. In addition, an increase of the basicity index leads to a strong drop in the swelling behaviour that is eliminated for basicity indexes close to 0.6 [75]. This is consistent with previous studies indicating the basicity index between 0.4 and 0.6 as lowering the melting point slags formed and corresponded to the highest reduced swelling index [76].

The pellets dimensions ranged between 1.14 and 1.72 cm (Fig. 6).

The surface aspect of the pellets is shown in Fig. 7.

As can be seen in Fig. 7, the pellets show a very different aspect in terms of granulometry and granules distribution with the finest aspect revealed for the medium size pellets (1.36 cm).

The pellets density was 2.6, 3.5 and 3.4 for the pellets with 1.14, 1.36 and 1.72 cm in diameter respectively.

The pellets' surface was statistically analysed in order to measure the medium size of the surface pores as shown in Fig. 8.

The distribution of the pores size is shown in Fig. 9.

The pores dimensions tend to decrease from the larger pellet to the medium one to increase again for the pellet with the smallest diameter. It is believed that both density and porosity as well as the pellets strength is largely influenced by the starting particles to be pelletized [77]. This obviously has large influence on the further reduction behaviour. The systematic analyses of porosity in this class of pellets reduced in different temperature conditions can be observed in Ref. [78].

The compressive resistance of the pellets is shown in Fig. 10.

The strength of the pellet is maximum for the medium size ones (the pellets with the highest density) then it decreases with the density for the biggest size and decrease again for the smallest diameter ones. This difference with respect to the pellet density is due to the effect of the pores that embrittle the pellets behaviour especially in the case of the smallest diameters. The aspect of the pellets after tests is shown in Fig. 11.

In general, pellets with a basicity close to 0.6 are characterized by high strength but high levels of shattering. This is accompanied with a high reduction swelling behaviour and a large presence of surface cracks. This is consistent with previous studies indicating a basicity close to 0.6 as an optimal condition for high strength pellets [79].

Some examples of the reduction curves are shown in Fig. 12.

As a general behaviour, by varying the composition of the reducing gas, the influence of the different input parameters largely changes from the point of view of both processing parameters and chemic-physical properties of the reduced pellets. The reduction through total hydrogen shows the fastest reduction behaviour with total time to reduction mainly influenced by the temperature and by the chemical properties of the employed industrial pellets. These pellets, particularly designed for hydrogen direct reduction show a very fast reduction in the time for metallization as increasing the gas temperature from 800 °C to 1000 °C [80].

The aspect of the pellets after hydrogen reduction is shown in Fig. 13.

The dimensions evolution and the weight of the pellets after and before the reduction at 950 °C and 1000 °C is shown in Table 2.

As an example, Fig. 14 shows the aspect of the pellets with different size in the unreduced and reduced conditions.

The main observable results are that as the hydrogen reduction is performed, porosity increases and the pores dimensions increase.

The porosity variation as a function of the initial pellets diameter is shown in Fig. 15.

The biggest pores in the center of the pellets tend to increase more with respect to the smallest ones, as shown in Fig. 16.

The whole database is visible as supplementary material. Here all the studied conditions and the resulting data are available.

The developed database was analysed through the multi objective optimization software (modeFrontier). First of all, it was underlined the weight that each single input parameter has on each corresponding output. This aspect can be viewed through the so called scatter matrix in Fig. 17.

By considering the time to 95 % of reduction it is clear how the main influencing factor is the pellet diameter, then the pellet density (all with a direct correlation) and the gas temperature and the pores size (with an inverse correlation), the less influencing factor is the pores tortuosity (with a direct correlation).

As a general behaviour, as the pellets dimension varies the effect of density is different. If the pellet has a high density, the pellets' diameter effect decreases, the contrary is revealed in the case of large particles for which the effect of the density is reduced.

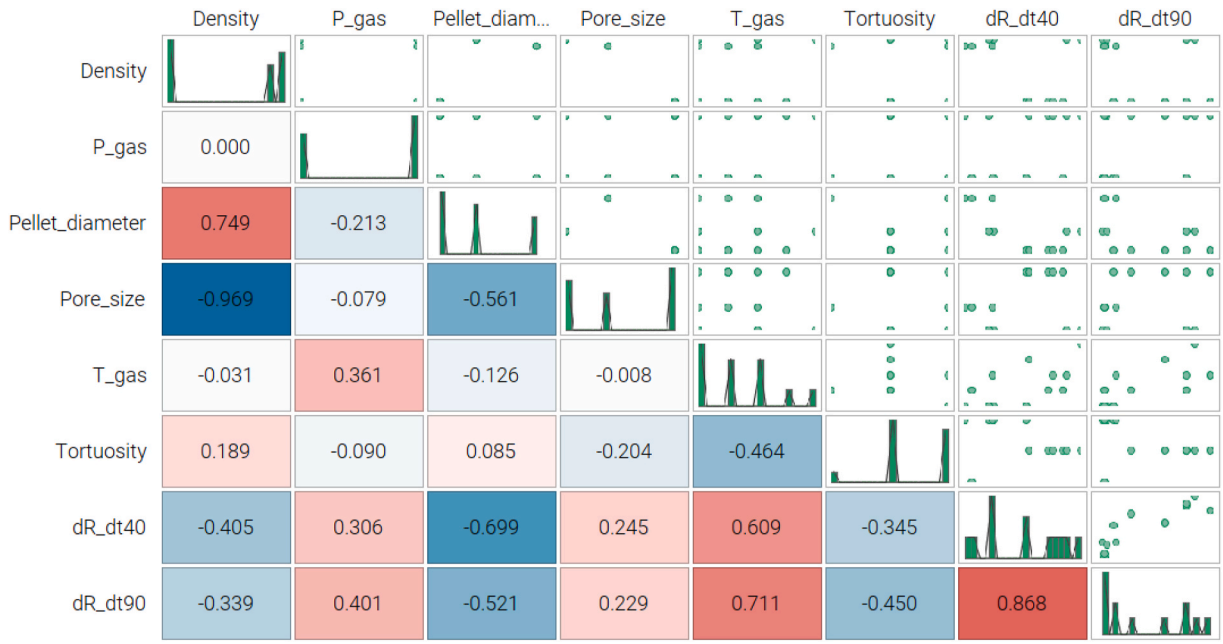

Fig. 21. Scatter matrix considering dR/dt_{90} as the only output parameter.

The relationships between the time to 95 % reduction and the input parameters are shown in Fig. 18.

So, obviously, the time needed to reach 95 % of reduction is first of all dependent on the surface pores size. The larger these pores are, the faster the pellets can reduce. This is obviously dependent on the pellet density describing the behaviour of pores in the pellets bulk, in fact, as the pellet density increases the time to reduction increases. For a single pore, also the pores tortuosity influences the time to reduction because at the same pores size the time to 95 % reduction increases as the tortuosity increases. In the case of high pellets density the reactions of reduction are known to evolve stepwise that can be modelled through a shrinking core description. In this case the reduction time is higher and is directly proportional to the pellets dimensions. This aspect can be particularly underlined for the pellets of 1.72 and 1.36 mm in diameter that having a very similar density reduce with a direct proportion to their diameter. In the case of low density pellets, the gas diffuses very fast and the reduction times are significantly reduced. So, the time to 95 % reduction is lower for all those pellets with low density that in this particular case are also characterized by an intermediate surface pores dimensions.

Taking into account the tortuosity factor inside the pellets, the time to reduction increases as the tortuosity of the pores increases, as the porosity decreases (increased density) and the pores dimensions decrease. This is why from the energy point of view, these parameters largely lead to variations in the entropy generated during all the reduction phases [81]. Entropy starts to increase in the first stages of the direct reduction as a consequence of the heat transfer between the heated hydrogen and the pellets surface. The entropy tends to increase as the porosity and the gas ration decrease because of the reduction of the exchange surfaces. The entropy generation is then further increased as the pores tortuosity increases. This is due to the fact that tortuosity is an obstacle for the gas flowing and for its ideal path inside the pellet. Basically, this reduces the overall gas diffusion and, as a consequence, its reduction effect.

Entropy generation has two main contributes from the chemical reactions and from the mass transfer. By considering the entropy generation contributions as separate, as the porosity in the pellet decreases the entropy generation due to heat transfer increases. Here, the entropy increases immediately during the first stage of reduction because of the temperature gradient between the pellet surface and the heated hydrogen. After this, entropy decreases up to a steady state and it remains constant because the thermal gradient tends to decrease as the reduction process proceeds.

By considering pellets where the porosity increases, the resistance to the gas penetration inside the pellets decreases. As a consequence of the easy gas penetration, the entropy generation decreases. The second contribution is the entropy generation due to the chemical reactions. Here, the entropy generation tends to rapidly increase in the first reaction stages but in this case it decreases up to a zero value as the chemical reactions proceeds. Also in this case, as the porosity of the pellets increases, the entropy generation decreases. Obviously, the entropy generation leads to increased energy expenses for the overall reduction process [82].

The other contribution to the entropy generation comes from the mass transfer. This contribution shows a fast increase in the first stages of reduction and then it decreases up to a plateau value. In the case of high porous pellets, this contribution can approach the zero value after the peak increase because of the reduction to the gas penetration inside the pellets. Anyway, the entropy is never null because of the compositional gradient between the pellet surface and the not already reduced bulk. To give an idea of the total contribution, we can say that the highest effect is due to the heat transfer, an intermediate effect is due to the chemical reactions while the lowest effect is due to the mass transfer [83,84]. So, during the initial stages of reduction the process is controlled by both the chemical reaction and the gas diffusion while in the second stage of reduction the rate limiting step is the interfacial chemical reactions.

Now, let's go to examine the different stages of the hydrogen direct reduction. The first stage (rapid) of reduction is generally evaluated through the calculation of the dR/dt40 index. The dependence of the dR/dt40 parameter on the various inputs shows that it is mainly related to the gas temperature (direct proportionality), then to the pellet density and diameter (inverse proportionality), then to the pore size (direct proportionality) and finally to the tortuosity and gas pressure (inverse proportionality).

The dependence of the dR/dt40 parameter with respect to the different processing parameters is shown in Fig. 19.

The dR/dt_{90} is largely related to the dR/dt_{40} parameter as it will be discussed later.

By observing the kinetics parameters, it is clear how they are firstly

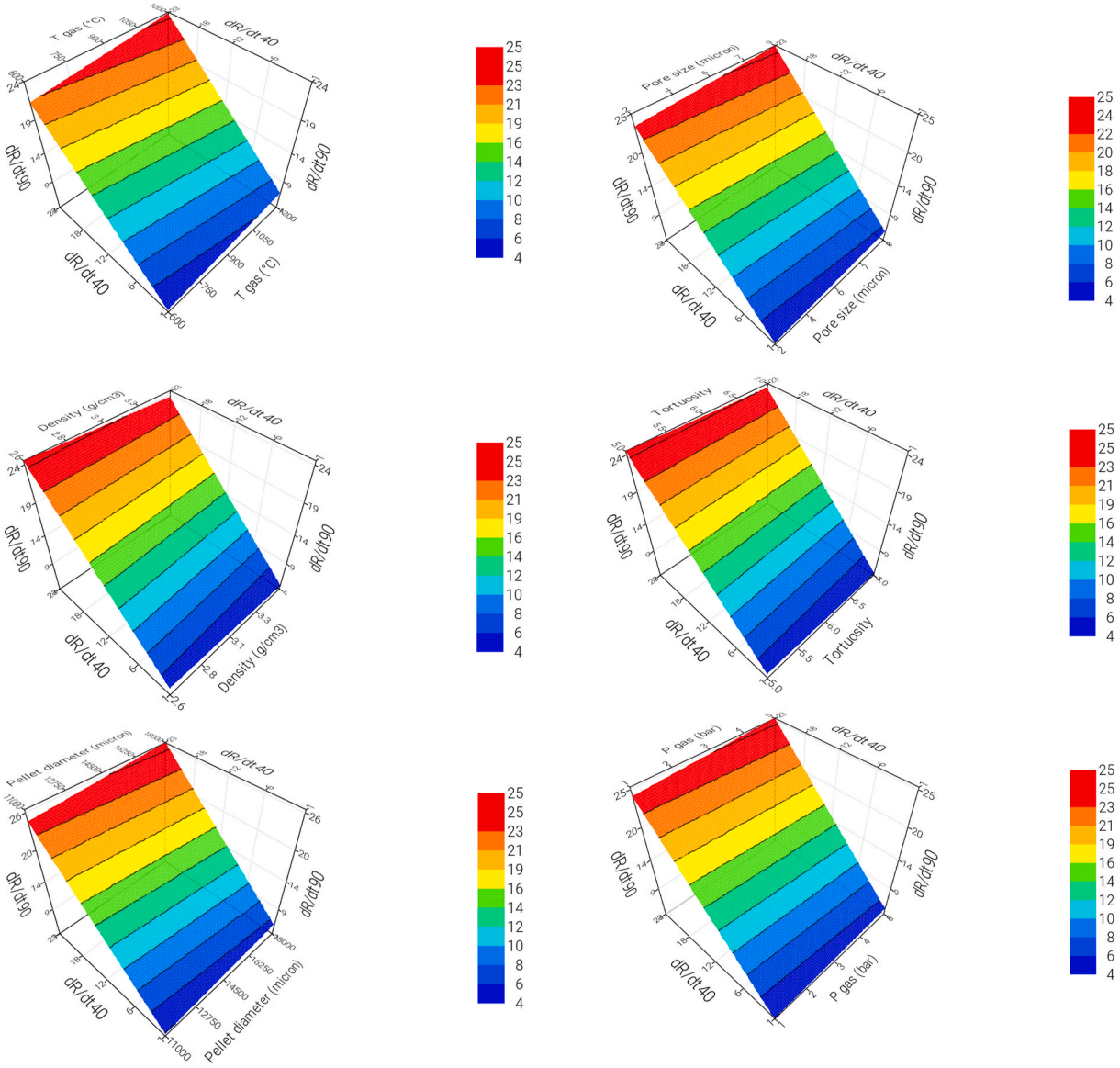

Fig. 22. dR/dt90 as a function of dr/dt40 and the other input parameters.

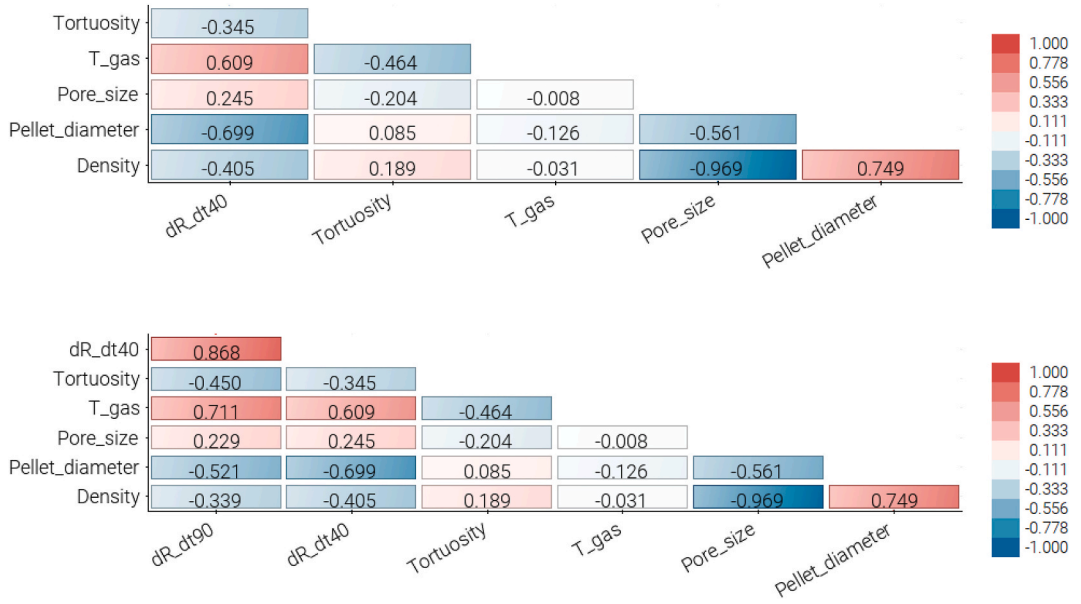

Fig. 23. Correlation matrix among the different parameters.

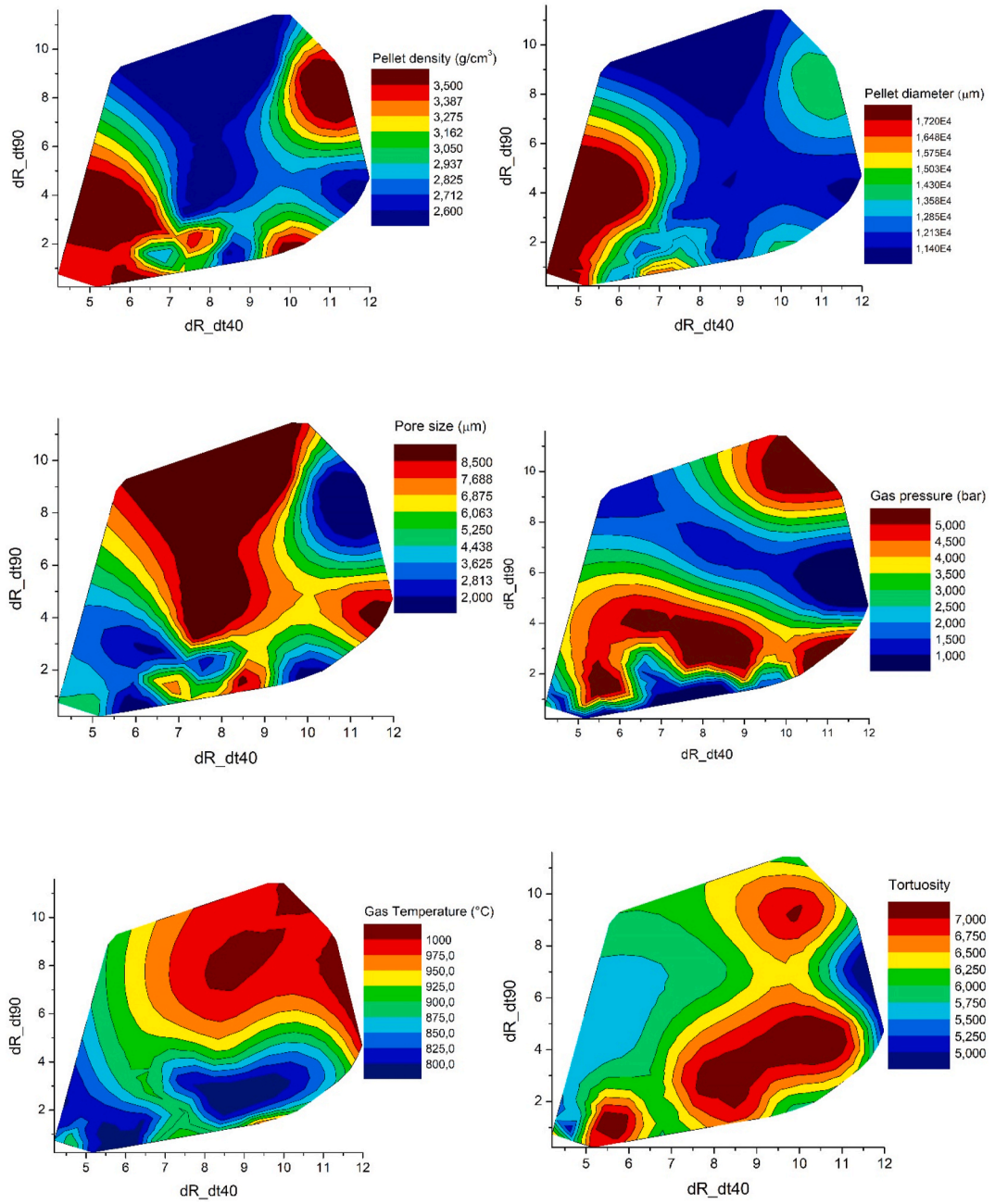

Fig. 24. Relationship among the two reduction indexes and the different pellets and processing parameters.

influenced by pellets diameter and density (with inverse proportionality) then they are influenced by temperature and pore size (with direct proportionality) and finally by tortuosity and gas pressure (with inverse proportionality).

The first kinetic parameter behaviour as a function of the various inputs is shown in Fig. 20.

By observing the behaviour of the pellets reduction in terms of the kinetic constant variations, in the case of hydrogen direct reduction a hierarchy of phenomena can be underlined all determining the overall reduction in the time and space domains [85]. The phenomena developed in an industrial shaft furnace, in fact, depend on the kinetics behaviour and on the heat and mass transfer from the macroscopic scale to the atomic one (in different times) involving catalytic processes, diffusion, dissociation up to transfer of charges [31]. In addition, these phenomena are characterized by a non-linear interplay among them. This needs the employment of very different characterization and modelling instruments to be addressed. So, the macroscopic gas transportation and diffusion plays different roles at different scales of the process that is strictly related to the pellets microstructure and chemical-physical properties [86]. Al microscale, the process kinetics are determined by both micro and atomic scale phenomena because of the different oxides involved transformations, of the crystal defects and of the local compositions [87].

Given a kinetic behaviour of the reduction process due to the processing conditions and pellets composition as well as density and porosity size, tortuosity largely influence the reduction. First of all, as tortuosity increases, the kinetic constants decrease. This is due to the fact that in the same conditions of pressure and temperature and then of mass transfer, less hydrogen atoms interact with the material bulk as the tortuosity increases. So, the final effect is that for very tortuous pellets, the kinetics of the reactions are reduced (both again in the time and space domains).

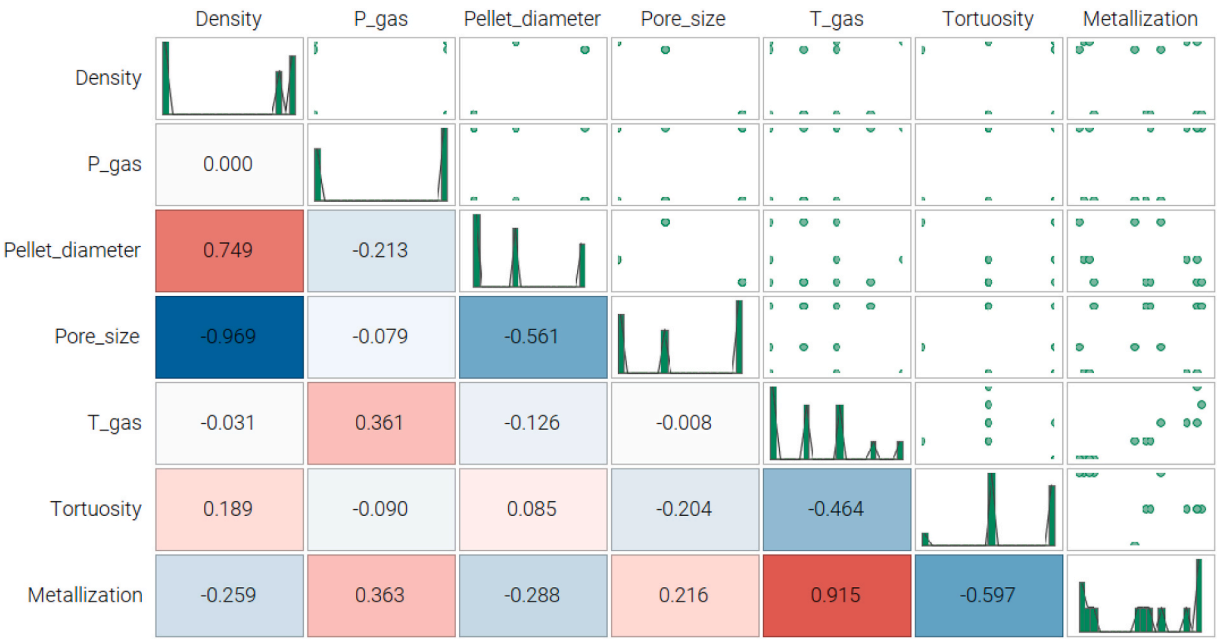

Fig. 25. Scatter matrix considering metallization degree as the only output parameter.

The tortuosity factor has also large implications of the overall entropy behaviour and then on the energy input during the direct reduction process [88]. In addition, the tortuosity is more influencing as the pellet diameter increases.

Generally, as the tortuosity increases, the entropy generation and then the energy consumption increase. In addition, the entropy generation tend to increase with a non-linear behaviour especially in the final stages of reduction as the tortuosity of the pellets is very pronounced.

A particular discussion is needed for the dR/dt_{90} behaviour. Now, it is largely influenced by the dR/dt_{40} (that is referred to the first linear stage of the reduction curve) and obviously by the pellets properties that vary during the reduction process as the oxides transformations take place. In this view it was defined a new scatter matrix taking into account also dR/dt_{40} as input parameter by considering only dR/dt_{90} as output. The results are shown in Fig. 21.

It is immediately clear how the dr/dt_{90} ir related to the dR/dt_{40} with a direct proportionality so the time to reach the deep metallization decreases as the time of the first reduction stages decrease. Then dR/dt_{90} is mainly influenced by the pellet density and the pellet diameter (with inverse proportionality), then by the gas temperature and pores size (with direct proportionality), then by the tortuosity (with inverse proportionality) and finally by the gas pressure (with direct proportionality). This means that the final stage of the reduction is first of all influenced by the volume to be reduced and then by the gas path inside the pellet. The behaviour of the dR/dt_{90} with the various inputs is shown in Fig. 22.

Another factor influencing the ongoing reduction behaviour is the surface conditions; in the case of very small surface pores and then a denser surface, a very hard iron layer form on the surface. If this very hard dense iron layers develop during reduction this strongly tends to lower the reduction rate. This, in fact, limits the gas penetration inside the pellet by reducing the effect of the hydrogen. In the case of very hard layers rapidly formed on the surface the reactions tend to be governed by the solid-state diffusion. The gas penetration through the hard iron layers can be improved at higher levels of temperature. The inconvenience is due to the softening of the pellets as the temperature increases. This can reduce the pellets porosity by consequently reducing the reduction rates.

So, the behaviour of the two indexes (referring to two different sections of the reduction curves) are completely different in terms of dependence on the processing parameters; even if the dR/dt_{90} index is strictly related to the dR/dt_{40} one. The different dependence on the pellets properties and on the processing parameter is due to the fundamental aspect that they refer to different transformations taking place at different reduction steps (different oxides reduction) and to the fact that the material composition and pellets shape tends to vary as the reduction process is carried out. So, the two indexes are indicative of how the reduction of the different iron oxides are going to be reduced condition by condition. So, the dependence of the single index on the different processing parameters changes. The different stages of reduction indicate the behaviour of different reactions taking place in the pellet, so, the absolute values and the influence of the input parameters vary. As going from the dR/dt_{40} to the dR/dt_{90} index, the effect of all the processing parameters decreases while it increases the dependence of dR/dt_{90} on dR/dt_{40}. As a matter of fact, the dependence of the dR/dt_{90} parameter on the dR/dt_{40}, as shown in the scatter matrix is very high (0.758). So, by looking at the correlation matrix among the different parameters (Fig. 23), it is clear how the correlation between each reduction index and each processing parameter varies.

That actually can be visualized through the 3D maps in Fig. 24.

Here it is clear how the temperature is fundamental in the final stage of the reduction in order to gain a complete metallization of the pellets. Tortuosity reduces the metallization behaviour when reaching high values. Pore size increase favours both the indexes, while pellet diameter leads to a reduction of the metallization rate. This is mainly due to the effect of temperature whose increase leads to improvement of the driving force for diffusion in the inner layers of the pellets. Obviously, as already mentioned, the pore size is very influencing the dR/dt_{40} index and it has lower influence on the final stages of reduction. This is due to the not-negligible aspect that the pores dimension and pores geometry tend to modify as the reduction proceeds. So, in the final stages of reduction the pores from which the gas continues to penetrate the pellet are different from the beginning of the process. By considering the entropy generation and then the energy consumption, the peak is reached with inverse proportionality to porosity and pores size. After this, pores tend to increase in dimension and then the entropy generation decreases. So, also the energy consumption tend to decrease as the pores dimensions vary by going from dR/dt_{40} to dR/dt_{90}.

The final aspect that was analysed was the degree of metallization of the pellets in different conditions. Here, the parameter absolutely most

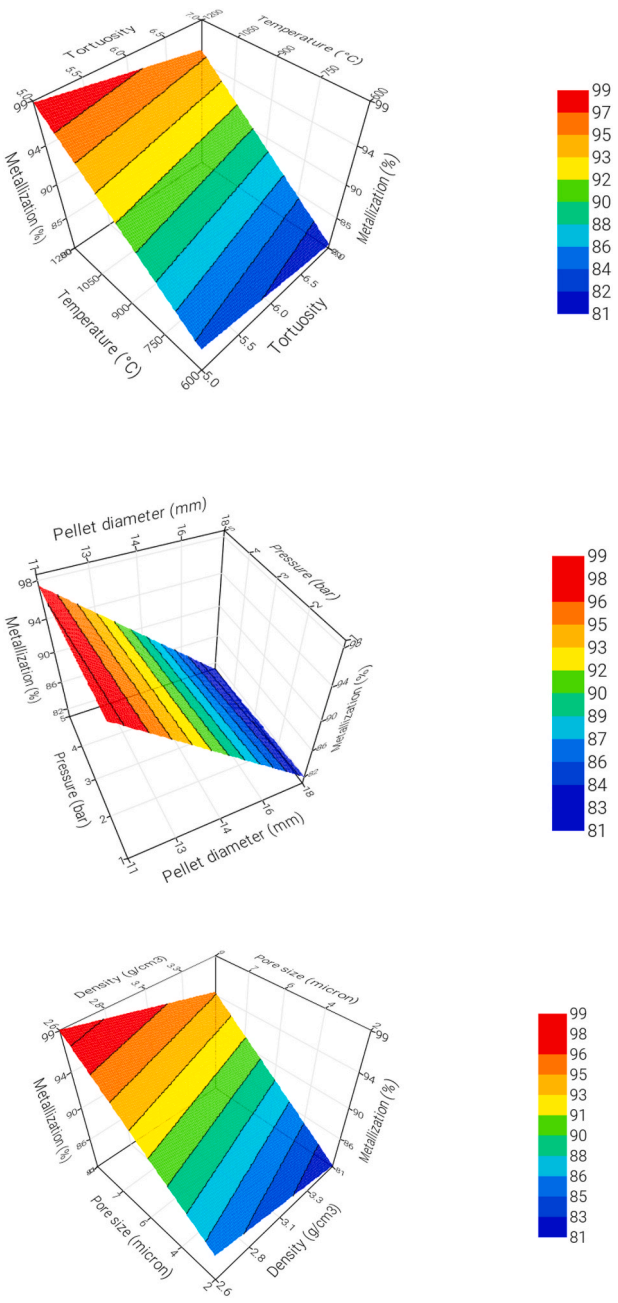

Fig. 26. Pellet diameter as a function of the different input parameters.

influencing the metallization behaviour is the reduction temperature (Fig. 25).

The metallization degree as a function of the different input parameters is shown in Fig. 26. The metallization degree is dependent on temperature, then on tortuosity, then on gas temperature and pellet diameter and finally on density and pore size.

Given the provided results of the present research, it can be stated that first of all the same pelletizing procedure leads to different shaped pellets with various densities and porosity geometry and distribution. This immediately has consequences on the strength behaviour of the pellets that results fundamental during the processing operations in the industrial direct reduction shaft furnaces. As a matter of fact, high compressive strength is required in order to avoid the collapse of the pellets in the shaft by retaining a high porosity for the gas penetration during the reduction. Obviously, all the physical and compositional properties of the starting pellets have severe influences on the reduction behaviour. Now, different processing parameters were taken into account to evaluate the reduction behaviour in different conditions. As a matter of fact, the time to 95 % reduction is mainly influenced by the pellet diameter and density and then by the gas temperature. This behaviour is obviously very similar to that of the reduction rates even if the rate of reduction in the last stages of the process is largely influenced by the rate of reduction in the first stages. This is also confirmed by the kinetics behaviour analyses that remarks the aspect related to the porosity, pores size and distribution and tortuosity as fundamental aspect in governing the reduction behaviour of industrial pellets in hydrogen atmosphere.

4. Conclusions

The paper presents the main results on the hydrogen direct reduction of industrial pellets performed by employing various processing conditions. The analysed pellets had an intermediate basicity index (0.52) and low different types of non-ferrous oxides. The pellets were selected in terms of their mean diameter. By considering different pellets, the surface morphology and the surface porosity resulted very different. This had a remarkable effect on the compressive strength that is related to the pellets' density and porosity geometries. Obviously, this influenced the reduction behaviour under hydrogen atmosphere performed at various temperatures and different pressures. In particular, for all the temperatures and pressures, employed during the experiments, as the pellet diameter increases the reduction time increased. The analyses of the weights that each single parameter has on the time to reduction and on the rate and kinetics of the reduction allowed to conclude that, the time to 95 % reduction is mainly influenced by the pellets diameter and density and then by the reduction temperature. The rate of reduction in the first stages is mainly influenced by the reduction temperature and then by the pellets physical properties. The kinetic constants show an intermediate behaviour.

Declaration of competing interest

The authors declare that they have no known competing financial interests or personal relationships that could have appeared to influence the work reported in this paper.

Acknowledgments

Authors would like to thank the Italian Ministry for University and Research (MUR) for the fundings provided under the Grant "Low environmental impact fuels for metallurgical industries- 2022P3PJXN".

Appendix A. Supplementary data

Supplementary data to this article can be found online at https://doi.org/10.1016/j.ijhydene.2023.11.040.

References

[1] https://worldsteel.org/steel-topics/statistics/world-steel-in-figures-2022/.
[2] Cavaliere P. Clean ironmaking and steelmaking processes efficient technologies for greenhouse emissions abatement. 2019. https://doi.org/10.1007/978-3-030-21209-4.
[3] Öhman A, Karakaya E, Urban F. Energy Res Social Sci 2022;84:102384. https://doi.org/10.1016/j.erss.2021.102384.
[4] Souza Filho IR, Springer H, Ma Y, Mahajan A, Caûe da Silva C, Kulse M, Raabe D. J Clean Prod 2022;340:130805. https://doi.org/10.1016/j.jclepro.2022.130805.
[5] Patisson F, Mirgaux O. Metals 2020;10(7):922. https://doi.org/10.3390/met10070922.
[6] Guo Dabin, Zhu Liandong, Guo Sheng, Cui Baihui, Luo Shipeng, Laghari Mahmood, Chen Zhihua, Ma Caifeng, Zhou Yan, Chen Jian, Xiao Bo, Hu Mian, Luo Shiyi. Fuel Process Technol 2016;148:276–81. https://doi.org/10.1016/j.fuproc.2016.03.009.
[7] Valipour MS, Motamed Hashemi MY, Saboohi Y. Adv Powder Technol 2006;17(3):277–95.
[8] Mousa EA, Babich A, Senk D. Steel Res Int 2013;84(11):1085–97. https://doi.org/10.1002/srin.201200333.

[9] Ranzani da Costa A, Wagner D, Patisson F. J Clean Prod 2013;46:27–35. https://doi.org/10.1016/j.jclepro.2012.07.045.
[10] Zhang Yujie, Yue Qiang, Chai Xicui, Wang Qi, Lu Yuqi, Ji Wei. J Clean Prod 2022;361:132289. https://doi.org/10.1016/j.jclepro.2022.132289.
[11] Scharm C, Küster F, Laabs M, Huang Q, Volkova O, Reinmoller M, Guhl S, Meyer B. Miner Eng 2022;180:107549. https://doi.org/10.1016/j.mineng.2022.107459.
[12] Kazemi M, Pour MS, Sichen D. Metall. Met. Trans. 2017;B48:1114–22. https://doi.org/10.1007/s11663-016-0895-3.
[13] Metolina P, Ribeiro TR, Guardani R. Int J Miner Metall Mater 2022;29(10):1908. https://doi.org/10.1007/s12613-022-2487-3.
[14] Meshram A, Govro J, Omalley RJ, Sridhar S, Korobeinikov Y. Metals 2022;12:2026. https://doi.org/10.3390/met12122026.
[15] Ribeiro TR, Ferreira Neto JB, Rocha Poco JG, Takano C, Kolbeinsen L, Ringdalen E. ISIJ Int 2022;62(3):504–14. https://doi.org/10.2355/isijinternational.ISIJINT-2021-472.
[16] Geng S, Zhang H, Ding W, Yu Y. Metalurgija 2018;57(4):219–22.
[17] Spreitzer D, Schenk J. Steel Res Int 2019;90(10):1900108. https://doi.org/10.1002/srin.201900108.
[18] Ribeiro TR, Ferreira Neto JB, Rocha Poco JG, Takano C, Kolbeinsen L, Ringdalen E. ISIJ Int 2021;61(1):182–9. https://doi.org/10.2355/isijinternational.ISIJINT-2019-477.
[19] Loder A, Siebenhofer M, Bohm A, Lux S. Clean. Eng. Technol. 2021;5:100345. https://doi.org/10.1016/j.clet.2021.100345.
[20] Cavaliere P. Hydrogen assisted direct reduction of iron oxides. 2021. https://doi.org/10.1007/978-3-030-98056-6.
[21] Zaini IN, Nurdiawati A, Gustavsson J, Wei W, Thunman H, Gyllenram R, Samuelsson P, Yang W. Energy Convers Manag 2023;281:116806. https://doi.org/10.1016/j.enconman.2023.116806.
[22] Liu Qian, Zhao Ying-jie, Huang Yi, Pei Feng, Cui Yang, Shi Li-juan, Chang Li-ping, Yi Qun. Fuel 2023;331:125862. https://doi.org/10.1016/j.fuel.2022.125862.
[23] Chang Yifan, Wan Fang, Yao Xilong, Wang Jianxin, Han Yunfei, Li Hui. Energy Rep 2023;9:3057–71. https://doi.org/10.1016/j.egyr.2023.01.083.
[24] Choi Wonjae, Kang Sanggyu. J Environ Manag 2023;335:117569. https://doi.org/10.1016/j.jenvman.2023.117569.
[25] Lopez G, Farfan J, Breyer C. J Clean Prod 2022;375:134182. https://doi.org/10.1016/j.jclepro.2022.134182.
[26] Rukini A, Rhamdhani MA, Brooks GA, Van den Bulck A. J. Sustain. Metall. 2022;8:1–24. https://doi.org/10.1007/s40831-021-00486-5.
[27] Bai Y, Mianroodi JR, Ma Y, Kwiatkowski da Silva A, Svendsena B, Raabe D. Acta Mater 2022;231:117899. https://doi.org/10.1016/j.actamat.2022.117899.
[28] Zhao Zichuan, Tang Jue, Chu Mansheng, Wang Xindong, Zheng Aijun, Wang Xiaoai, Yang Li. Int. J. Minerals 2022;29(10):1891–900. https://doi.org/10.1007/s12613-022-2494-4.
[29] Wang Zc, Chu Ms, Liu Zg, et al. J Iron Steel Res Int 2012;18:7–12. https://doi.org/10.1016/S1006-706X(12)60144-7.
[30] Li Shuo, Zhang Huili, Nie Jiapei, Dewil Raf, Jan Baeyens, Deng Yimin. Sustainability 2021;13:8866. https://doi.org/10.3390/su13168866.
[31] Ma Y, Souza Filho IR, Bai Y, Schenk J, Patisson F, Beck A, van Bokhoven JA, Willinger MG, Li K, Xie D, Ponge D, Zaefferer S, Gault B, Mianroodi JR, Raabe D. Scripta Mater 2022;213:114571. https://doi.org/10.1016/j.scriptamat.2022.114571.
[32] Salucci E, Ghosh S, Russo V, Grénman H, Saxén H. Comp. Aid. Chem. Eng. 2023;52:715–20. https://doi.org/10.1016/B978-0-443-15274-0.50114-1.
[33] Kazemi M, Glaser B, Sichen D. Steel Res Int 2014;85(4):718–28. https://doi.org/10.1002/srin.201300197.
[34] Bonalde A, Henriquez A, Manrique M. ISIJ Int 2005;45(9):1255–60. https://doi.org/10.2355/isijinternational.45.1255.
[35] Bai M-H, Long H, Ren S-B, Liu D, Zhao C-F. ISIJ Int 2018;58(6):1034–41. https://doi.org/10.2355/isijinternational.ISIJINT-2017-739.
[36] Ma Y, Souza Filho IR, Zhang X, et al. Int J Miner Metall Mater 2022;29:1901–7. https://doi.org/10.1007/s12613-022-2440-5.
[37] Ghadi AZ, Valipour MS, Vahedi SM, Sohn HY. Steel Res Int 2020;91:1900270. https://doi.org/10.1002/srin.201900270.
[38] Bhaskar A, Assadi M, Somehsaraei H Nikpey. Energies 2020;13(3):758. https://doi.org/10.3390/en13030758.
[39] Kirschen M, Hay T, Echterhof T. Processes 2021;9(2):402. https://doi.org/10.3390/pr9020402.
[40] El-Husseiny NA, El-Amir A, Mohamed FM, Abdel-Rahim S Th, Shalabi MEH. Int J Sci Eng Res 2015;6(7):1018–27.
[41] Abdel Hamid EM, Amin ShK, Sibak HA, Abadir MF. Int J Appl Eng Res 2018;13(6):3954–65.
[42] M Kirschen K Badr, Pfeifer H. Energy 2011;36(10):6146–55. https://doi.org/10.1016/j.energy.2011.07.050.
[43] Ali ML, Fradet Q, Riedel U. Steel Res Int 2022. https://doi.org/10.1002/srin.202200043.
[44] Sun G, Li B, Yang W, Guo J, Guo H. Energies 2020;13(8):1986. https://doi.org/10.3390/en13081986.
[45] Ma Y, Souza Filho IR, Zhang X, Nandy S, Barriobero-Vila P, Requena G, Vogel D, Rohwerder M, Ponge D, Springer H, Raabe D. Int J Miner Metall Mater 2022;29(10):1901. https://doi.org/10.1007/s12613-022-2440-5.
[46] Ali ML, Fradet Q, Riedel U. Steel Res Int 2022. https://doi.org/10.1002/srin.202200043.
[47] Cavaliere P, Perrone A, Silvello A. Metals 2021;11(11):1816. https://doi.org/10.3390/met11111816.
[48] Rechberger K, Spanlang A. Steel Res Int 2020;91(11):2000110. https://doi.org/10.1002/srin.202000110.
[49] Du Z, Liu J, Liu F, Pan F. Chem Eng J 2022;447:137588. https://doi.org/10.1016/j.cej.2022.137588.
[50] Man Y, Feng J-X. Powder Technol 2016;301. https://doi.org/10.1016/j.powtec.2016.07.057.
[51] Cavaliere P, Perrone A, Silvello A, Stagnoli P, Duarte P. Metals 2022;12(2):203. https://doi.org/10.3390/met12020203.
[52] Li Feng, Chu Mansheng, Tang Jue, Liu Zhenggen, Guo Jun, Yan Ruijun, Liu Peijun. Energy 2022;241:122922. https://doi.org/10.1016/j.energy.2021.122922.
[53] Ghalandari V, Rafsanjani HH. Chem. Chem. Technol. 2019;13(2):205–11. https://doi.org/10.23939/chcht13.02.205.
[54] Béchara R, Hamadeh H, Mirgaux O, Patisson F. Materials 2018;11(7):1094. https://doi.org/10.3390/ma11071094.
[55] Luo S, Zhou Y, Yi C. J Renew Sustain Energy 2013;5(6):063114. https://doi.org/10.1063/1.4839995.
[56] El-Geassy AA, Nas MI. ISIJ Int 1990;30(6):417–25. https://doi.org/10.2355/isijinternational.30.417.
[57] Li P, Li Y, Yu J, Gao P, Han Y. Int J Hydrogen Energy 2022;47(73):31140–51. https://doi.org/10.1016/j.ijhydene.2022.07.032.
[58] Fradet Q, Ali ML, Riedel U. Steel Res Int 2022. https://doi.org/10.1002/srin.202200042.
[59] Zuo H-B, Wang C, Dong J-J, Jiao K-X, Xu R-S. Int J Miner Metall Mater 2015;22(7):688. https://doi.org/10.1007/s12613-015-1123-x.
[60] Wang RR, Zhao YQ, Babich A, Senk D, Fan XY. J Clean Prod 2021;329:129797. https://doi.org/10.1016/j.jclepro.2021.129797.
[61] Zhang F, Zhu D, Pan J, Guo Z, Xu M. J Iron Steel Res Int 2021;28:1212–22. https://doi.org/10.1007/s42243-021-00620-3.
[62] Shi Yue, Zhu Deqing, Pan Jian, Guo Zhengqi, Lu Shenghu, Xu Mengjie. Powder Technol 2022;408:117782. https://doi.org/10.1016/j.powtec.2022.117782.
[63] Claremboux V, Kawatra SK. Miner Process Extr Metall Rev 2023;44:138–54. https://doi.org/10.1080/08827508.2022.2029431.
[64] Zare Ghadi A, Valipour MS, Biglari M. IJE Trans. B: Appl. 2018;31(8):1274–82. https://doi.org/10.5829/ije.2018.31.08b.16.
[65] Yi Man, Feng Junxiao. Powder Technol 2016;301:674–8. https://doi.org/10.1016/j.powtec.2016.06.013.
[66] Cavaliere P, Perrone A, Silvello A. Eng. Sci. Technol. 2016;19(1):292–312. https://doi.org/10.1016/j.jestch.2015.07.004.
[67] Cavaliere P, Perrone A, Silvello A. J Manuf Process 2015;17:9–27. https://doi.org/10.1016/j.jmapro.2014.10.005.
[68] Cavaliere P, Perrone A. Steel Res Int 2013;85(1):89–98. https://doi.org/10.1002/srin.201300027.
[69] Cavaliere P, Perrone A. Ironmak Steelmak 2013;40(1):9–24. https://doi.org/10.1179/1743281212Y.0000000019.
[70] Cavaliere P, Perrone A, Tafuro P, Primavera V. Ironmak Steelmak 2011;38(6):422–31. https://doi.org/10.1179/174328121 1Y.0000000034.
[71] P. Cavaliere, A. Perrone, D. Marsano, V. Primavera: Steel Res Int https://doi.org/10.1002/srin.202200791.
[72] Sesen MK. Scand J Metall 2017;30:1–7. https://doi.org/10.1034/j.1600-0692.2001.300101.x.
[73] Guo Yufeng, Liu Kuo, Chen Feng, Wang Shuai, Zheng Fuqiang, Yang Lingzhi, Liu Yajing. Powder Technol 2021;393:291–300. https://doi.org/10.1016/j.powtec.2021.07.057.
[74] Zhang Guo-Cheng, Luo Guo-Ping, Jia Peng-Fei, Wang Yi-Ci, Chai Yi-Fan. High Temp Mater Process 2021;40:193–203. https://doi.org/10.1515/htmp-2021-0027.
[75] Umadevi T, Kumar A, Karthik P, Srinidhi R, Manjini S. Ironmak Steelmak 2018;45:157–65. https://doi.org/10.1080/03019233.2016.1250043.
[76] Zhu Deqing, Chun Tiejun, Pan Jian, Zhang Jinliang. Int J Miner Process 2013;125:51–60. https://doi.org/10.1016/j.minpro.2013.09.008.
[77] Singh AK, Kumar S, Mishra B, et al. Canad. Metall. Quat. 2022;61(4):475–82. https://doi.org/10.1080/00084433.2022.2045530.
[78] P. Cavaliere, L. Dijon, A. Laska, D. Koszelov: Int J Hydrogen Energy https://doi.org/10.1016/j.ijhydene.2023.08.254.
[79] Shi Yue, Zhu Deqing, Pan Jian, Guo Zhengqi, Lu Shenghu, Xu Mengjie. Powder Technol 2022;408:117782. https://doi.org/10.1016/j.powtec.2022.117782.
[80] Cavaliere P, Perrone A, Marsano D. Powder Technol 2023;426:118650. https://doi.org/10.1016/j.powtec.2023.118650.
[81] Kim SH, Zhang X, Ma Y, Souza Filho IR, Schweinar K, Angenendt K, Vogel D, Stephenson LT, El-Zoka AA, Rezaei Mianroodi J, Rohwerder M, Gaulta B, Raabe D. Acta Mater 2021;212:116933. https://doi.org/10.1016/j.actamat.2021.116933.
[82] Wang R, Zhao Y, Babich A, Senk D, Fan X. Powder Technol 2022;407:117654. https://doi.org/10.1016/j.powtec.2022.117654.
[83] Guo D, Hu M, Pu C, Xiao B, Hu Z, Liu S, Wang X, Zhu X. Int J Hydrogen Energy 2015;40(14):4733–40. https://doi.org/10.1016/j.ijhydene.2015.02.065.
[84] Mirzajani A, Ebrahim H, Nouri SMM. Braz J Chem Eng 2018;35(3):1019–28. https://doi.org/10.1590/0104-6632.20180353s20170178.
[85] Bai M, Long H, Li L, Liu D, Ren S-B, Zhao C-F. J. Cheng 2018;43(32):15586–92. https://doi.org/10.1016/j.ijhydene.2018.06.116.
[86] Hammam A, Li Y, Nie H, Zan L, Ding W, Ge Y, Li M, Yu M Omran Y. Mining Metall. Explor. 2021;38(1):81–93. https://doi.org/10.1007/s42461-020-00317-3.
[87] Xie DG, Wang ZJ, Sun J, et al. Nat Mater 2015;14:899–903. https://doi.org/10.1038/nmat4336.
[88] Sundberg R. Reduction of iron oxides with hydrogen, master degree thesis. Abo Akademy University; 2021.